International Journal of Science and Research (IJSR)
ISSN: 2319-7064
Impact Factor 2024: 7.101

Characterization and Applications of Laser-Produced Plasmas in Elemental Analysis and Tokamak Research: A Review

Hosam Hegazy

Department of Physical Sciences, College of Science, Jazan University, P. O. Box 114, Jazan 45142, Kingdom of Saudi Arabia
E-mail: hhegazy@ jazanu.edu.sa

Abstract: ***This review article provides a comprehensive overview of laser-produced plasmas (LPPs) and their diverse applications, particularly focusing on Laser-Induced Breakdown Spectroscopy (LIBS) and its relevance to elemental analysis and Tokamak research. It discusses the fundamental processes of laser-matter interaction, including plume formation, ablation mechanisms, and plasma generation, in detail. Key experimental parameters that influence LPP characteristics, such as laser fluence, pulse width, wavelength, and ambient gas conditions, are thoroughly examined. The article also delves into the spectroscopic characterization of LPPs, outlining methods for determining plasma temperature and electron density, as well as crucial criteria for ensuring local thermodynamic equilibrium (LTE) and optical thinness. Furthermore, the review highlights the analytical capabilities of LIBS for elemental analysis, discussing sensitivity, matrix effects, and advancements such as double-pulse LIBS. Finally, it explores the significant role of LPP in Tokamak diagnostics and the diagnosis of the plasma-facing components, emphasizing the use of laser blow-off (LBO) for atomic beam generation and the application of spectroscopic techniques for plasma parameter measurements in fusion devices.***

Keywords: Laser-Induced Breakdown Spectroscopy, LIBS, Laser-produced Plasma (LPP), Plasma Parameters Temperature and Density, Optical Emission Spectroscopy (OES), Laser Blow-off (LBO), Plasma Facing Components (PFCs), Tokamak, Fusion.

1. Introduction

Laser produced plasmas are considered a versatile and widely applied technique in various fields, such as elemental analysis, material processing, thin film deposition and Tokamak research and related diagnostics [1-7]. When a high-power laser pulse is focused onto a material target (solid, liquid, gas, aerosols, and thin film), the intensity at the focal spot produces rapid local heating and intense material evaporation followed by plasma formation. The interaction between a laser beam and the target is a complex process influenced by many characteristics of both the laser and the material itself. Various factors affect ablation of material, including the laser pulse width, its spatial and temporal fluctuations, as well as power instability. The mechanical, physical and chemical properties of the target material also play a significant role in laser-induced ablation.

The plasma induced by nanosecond lasers is used in thin film deposition of traditional and new materials [4]. Pulsed laser deposition (PLD) had been proven to be an easy and highly efficient technique for producing high quality thin films [8-10], and it can be conducted in a reactive gas environment. The flux of sputtered material reacts with the environment gas molecules before deposition [11-13]. However, the plasma produced by short-duration laser pulses is an efficient technique for the production of nano-scale particles [14-16].

In recent years, there has been a growing interest in both the fundamental understanding of laser produced plasma or laser induced plasmas (LIPs) and the development of their practical applications [17-19]. Optical emission spectroscopy (OES) is commonly employed for the elemental analysis of target materials, from which the luminous plasma is generated. Additionally, it can be applied to determine key plasma parameters such as temperature, electron density and atomic density within the LIP [20]. Laser Induced Plasma Spectroscopy (LIPS), also commonly referred to as Laser Induced Breakdown Spectroscopy (LIBS), falls under the category of analytical techniques based on atomic emission. A LIP system functions as a form of atomic emission spectroscopy (AES), utilizing laser generated plasma as the source of vaporization, atomization, and excitation.

A LIPS measurement involves the generation of a -plasma plume on a target surface using high- power laser pulses, followed by the spectral analysis of the emitted radiation. The interaction between intense laser light and matter has been extensively studied in plasma physics, materials science, chemical physics, and analytical chemistry [21]. A high intensity laser beam focused on a target - whether solid, liquid, or gas-can dissociate, excite, or ionize its atomic species, leading to plasma formation. This plasma expands either into a vacuum or an ambient gas, depending on experimental conditions. Laser-matter interaction can trigger various processes, including material ablation, target acceleration, high-energy particle emission, parametric instabilities, and radiation spanning from the visible to hard X-rays, depending on the laser intensity [22].

This review outlines the fundamentals of laser–target interactions and the resulting plasma formation. It also addresses plasma characterization and its application in elemental analysis and tokamak-related research.

Plume Formation Process: Overview

LIPS in solids involves several sequential phenomena, including laser–solid interaction, ablation of surface material, and plasma formation (breakdown) [23]. As outlined by J.M. Vadillo and J.J. Laserna, the process begins with the reflection or absorption of pulsed radiation energy by the solid [23]. At moderate irradiance level (below ~10^6 W cm^{-2}), the absorbed energy is rapidly converted into heat

leading to material vaporization as the local temperature approaches the material's boiling point. This explanation behavior is typical of lasers operating in the nanosecond regime. The ejection of particles forms a vapor plume in front of the surface, which can condense into submicron-sized droplets. As irradiance increases, the laser beam induces strong heating, ionization, and plasma formation, along with a complex set of thermal, mechanical, and electromagnetic processes in both the solid and the ejected material [24].

The dynamical evolution of laser plumes is initiated by a rapid expansion of photo-ablated fragments. As the plume cools, the formation of polyatomic aggregates and clusters is facilitated. Subsequently, the ablated material is redeposited, along with molten material, around the crater, the morphology of which depends on the sample properties and laser parameters such as fluence, wavelength, and pulse width.

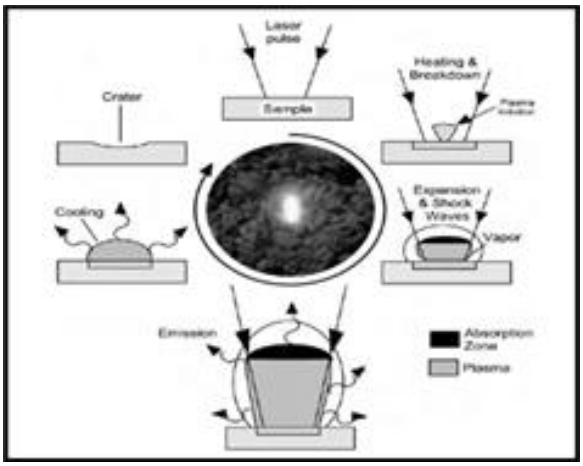

Figure (1): Schematic illustration of the main processes involved in laser-induced plume formation [23].

The detection step in LIPS is common to many other techniques based on optical emission spectrometry. However, due to the high electronic temperature of laser plasmas, time-resolved detection is required to enhance sensitivity. It must be taken into account that during laser-target interaction, the electron density of the plasma is particularly high. Under these circumstances, spectra are characterized by a non-specific continuum emission resulting from ion–electron interactions (recombination and bremsstrahlung), where the ionic and atomic lines are superimposed. Once the plasma begins to cool, acquiring emission spectra during the plasma lifetime becomes feasible. In principle, the timing parameters (delay and integration times) are highly dependent on the element and the matrix, and must be optimized for each sample[23].

2. Experimental factors considered in lips measurements

Several factors related to the sample, the laser, or their mutual interaction significantly affect plasma formation processes and its behavior. Understanding these phenomena is essential to determine the optimal conditions for an experiment involving time and spatially-resolved solid analysis.

2.1 Laser Characteristics

2.1.1 Energy threshold effects (Laser Fluence)

For a laser plasma to be formed, the fluence (or irradiance) at the target must exceed a certain threshold value. As the sample must first be vaporized, a vaporization threshold must be attained. In this sense, three fluence thresholds can be identified: the damage threshold, the ablation threshold, and the plasma threshold.

(i) The damage threshold fluence is usually defined as the fluence needed to induce a surface modification observable under an optical microscope. Some features such as cracks, cleavages, voids, grain boundaries, steps, surface roughness, impurities or inclusions may significantly affect its value.

(ii) The ablation threshold fluence corresponds to the level at which material removal begins. The process initiates when the energy deposited on the target exceeds the latent heat of vaporization (L_v). The threshold fluence (F) is given by[25]:

$$F_{th} = \rho\, L_v\, a^{1/2}\, t\, L_v^{1/2} \quad (1)$$

Where ρ is the sample density, t is the laser pulse width, and a is the thermal diffusivity (a=K/ρc), with K and c being the thermal conductivity and specific heat, respectively. In general, material will be ablated by vaporization to a depth at which the input energy equals the vaporization energy.

(iii) The plasma threshold is the fluence required for optical breakdown of the vapor phase. Plasma thresholds measured by LIPS have been studied for a number of metals using ns-Nd:YAG pulses [26]. Fluence threshold values correlate reasonably well with thermal properties of the metals. These results are relevant for LIPS surface studies as the surface sensitivity should be limited by the crater depth at the breakdown threshold fluence. Consequently, best depth-resolved results are anticipated for low melting point metals with UV laser wavelengths.

2.1.2 Temporal Regime (Laser Pulse Width)

The explosive nature of laser- material interaction is not fundamentally deterministic and may not be predicted or controlled in advance [27]. Of particular interest for understanding the principles of laser-matter interaction is the study of the effects of laser pulse width on plasma formation [28].

For femtosecond pulse widths, the time scale is shorter than the electron cooling time, and the lattice is instantaneously heated, resulting in plasma formation and vapor phase expansion. Due to the short time range, thermal conduction into the target is neglected, explaining the low heat affected zone in femtosecond laser ablation.

In the picoseconds regime, it exists some electron cooling exists due to energy exchange with the lattice (heat conduction), and thus a melted zone is formed inside the

target. Although near the sample surface it is still possible to consider evaporation as a direct solid plasma transition.

In the nanosecond regime, the lattice and electron temperatures are being equilibrate due to the long pulse duration. The absorbed laser energy first heats the surface to the melting point, then to the vaporization temperature, and finally the particle is ejected from the sample. Metals require much more energy to vaporize than to melt. As calculated [29] for copper particles, the process of ejecting a vaporized particle is not thermodynamically favored: the energy needed to eject a melted particle is only approximately 2% of the energy required to evaporate the same mass. In brief, during the interaction of a nanosecond laser beam with a sample, the main source of energy losses is the heat conduction into the solid target. In this temporal regime, there is enough time for the thermal wave to propagate into the target and to create a relatively large melted layer and an extended heat-affected zone. In this case, evaporation occurs from the liquid metal, which makes precise material processing or modeling on the ablated mass very complex. The sample was completely drilled. In the fs regime, there is no trace of molten material around the crater. In the ps and ns regimes, molten material can be observed, due to the presence of a liquid phase which leads to unstable ablation as target material is removed in both the vapor and liquid phases. The effect is a recoil pressure that explosively expels the liquid.

Since the early 2000, there has been a significant increase in the number of articles addressing LIPS with ultra-short laser pulses [30-34]. In most of these studies, the rapidly decaying background emission in observed in the fs regime is emphasized in comparison to the ns regime, a feature that may eliminate the need for gated detectors in conventional LIPS setups. However, the excellent control over crater morphology and high reproducibility achievable in the fs regime offers promising potential for detailed LIPS surface characterization. Nevertheless, selective fractionation appears to persist, at least under moderate fluence conditions [32].

2.1.3 Laser wavelength effects

Different kinds of lasers are used in 1aser induced plasma spectroscopy, typically ranging from UV excimer lasers to infrared solid-state lasers. Amoruso et al. [35] evaluated the efficiency of the mechanisms of energy absorption in the plasma for visible and UV laser wavelengths during ablation of an aluminum sample. There are two dominant photon absorption processes in the aluminum vapor for visible and UV photons. One is inverse bremsstrahlung (IB) absorption, by which free electrons gain kinetic energy from the laser beam, thereby promoting plume ionization and excitation through collision with excited and ground state neutrals. The second mechanism is photoionization (PI) of excited species and, at sufficiently high laser intensity, multiphoton ionization (MPI) of excited or ground state atoms. The authors observed that the primary mechanism of laser absorption and ionization of the relatively cold neutral vapor formed by the leading edge of the ablating laser pulse depends strongly on the radiation wavelength. At $\lambda = 532$ nm, the ionization is mainly ascribed to electron-neutral IB processes, and consequent electronic ionization, whereas at $\lambda = 355$ nm, direct PI of excited states in the vapor seems to be the most effective process. However, the IB process is less efficient in the UV than in the visible part of the spectrum, because of the λ^3 dependence of IB on the laser wavelength. More precisely, the efficiency of the laser heating of the plasma by IB decreases with the square of the laser wavelength when the degree of ionization is low and as the cube of the wavelength when the ionization is extensive [35-36]. The efficiency of the IB photon absorption is such that the plasma acts as a shield for the laser radiation, completely preventing the last part of the beam pulse to reaching the target surface.

Sdorra et al. [37] compared the characteristics of plasma induced by infrared and UV laser wavelengths (fundamental and fourth harmonic of a Nd:YAG laser). Under the same pressure conditions (argon buffer gas) the UV wavelength was found to be more effective for mass ablation. Moreover, using the fourth harmonic, the crater dimensions -and hence the ablated mass- increased significantly. The amount of mass ablated was found to be almost independent of the type of buffer gas and the pressure value (ranging from 140 to 1000 mbar), indicating that radiation shielding is negligible at this wavelength. Regarding plasma temperature, the authors measured at the center of the plasma for both fundamental or the UV wavelengths. However, a more pronounced temperature drop was observed in the lateral regions for the UV-induced plasma. In conclusion, the authors evaluated the analytical results and observed that the emission signals obtained with the UV radiation were not linearly correlated with the analyte concentration, even after comparing the LIBS signal with reference lines. They suggested that the reduced analytical performance with UV wavelengths may be due to incomplete atomization of the ablated material, and demonstrated that linearity can be achieved when the ablated vapor is reheated by a second, independent IR pulse. However, different observations have been reported by Berman and Wolf [38], who compared the analytical results obtained in the detection of Ni in water by using either the fundamental Nd:YAG wavelength or its UV third harmonic. They observed that the UV generated spectrum exhibited lower continuum intensity, resulting in a better signal-to-noise ratio. After constructing the calibration curves for the same spectral lines, the one obtained with UV radiation showed a higher slope and enabled a lower limit of detection (LOD). These results are consistent with those of Ng et al. [39], who found that the main difference in the plasma plume generated by visible or ultraviolet laser of the same fluence lies in the T_e value, which is significantly lower in the UV case, while the N_e value remains approximately the same.

Cabalin and Laserna [40] found that the fluence threshold for plasma formation increases with decreasing wavelength. They measured the emission intensity of the atomic lines characteristic of various metals as a function of laser fluence and for different harmonics of a nanosecond Nd:YAG laser (fundamental, second harmonic, fourth harmonic). The authors observed a similar behavior across the three wavelengths and different metals: a linear increase of the line intensity followed by a saturation regime. Both the plasma formation thresholds and the saturation regimes were

shifted toward lower fluence values for IR wavelengths, while energy threshold values were higher for UV radiation. In discussing their results, the authors stated that reflectivity does not appear to be a significant factor at high fluence levels (i.e., above the threshold), as plasma formation substantially alters the surface properties of the target.

In general, the selection of laser wavelengths depends on the analytical objective. For example, Haisch et al. [41] chose to use the second harmonic of an Nd:YAG laser, rather than a higher-order harmonic, to sample particles deposited on a filter membrane used for separating colloids from their liquid solvent. In this case, the formation of a deep crater, which would have occurred with the use of the fourth harmonic, was intentionally avoided to prevent ablation of the membrane layer along with the collected particles.

2.1.4 Laser Coupling Efficiency (Plasma Shielding)

A considerable reduction in ablation efficiency, known as plasma shielding, may occur due to the formation of particulate material. Plasma shielding is long been recognized, [42-43], although the most comprehensive studies have been presented only recently [44-45]. Specific experimental parameters may influence the extent of the shielding effect. A detailed study [46] described the variation of the line intensities in laser-induced plasmas as a function of laser pulse energy and the lens-to-sample distance (LTSD). As expected, optimal reproducibility was achieved under conditions where shielding is minimized, resulting in higher line intensities. The effect of plasma shielding on laser ablation rates for metals has also been reported [47] for various metal targets. A linear increase of the mass ablation rates up to a cut-off value (i.e., a plateau) was observed. This behavior was also evident under vacuum conditions. Many authors have compared the theoretical and experimental ablation rates, concluding that at high fluencies, the measured ablation rates are only a fraction of the theoretical values. This is attributed to the negative impact of plasma shielding, which is often not considered in theoretical models [23]. This interpretation is consistent with studies that directly measured the ablated mass per single pulse [48].

2.2 Interval of Observation

Early stages of plasma evolution are characterized by the bremsstrahlung continuum emission, while subsequent stages reveal the characteristic spectral line patterns that enable LIBS plasma diagnostics and compositional analysis. It should be noted that although the continuum emission may hinder line detection, it should not be considered noise, as it results from a real physical process and cannot be removed through averaging. Due to its characteristics, the continuum background can only be minimized by triggering spectral acquisition with an appropriate delay after the laser pulse that initiates the plasma. However, at long delay times, the absolute intensity of line emission may become too low for effective detection. Therefore, the optimal balance between high line intensity and low background must be determined on a case-by-case basis. Depending on the ambient gas density and other experimental factors, the plasma lifetime may vary from a few ns to more than 40 □s [49] or even up to 70 □s [50a], depending on laser pulse energy.

Ciucci et. Al. [51] compared the time evolution of the plasma emission obtained by irradiating the same sample in air using, respectively, the fundamental wavelength of an Nd:YAG laser and the UV radiation of an excimer laser. They observed that in the case of UV excitation, the background emission -up to approximately 400 ns- initially dominated, after which atomic transitions began to appear against the continuum. The emission generated by NIR excitation exhibited characteristically longer durations, on the order of several microseconds. The time scales of the plasma emission induced by the two sources differ significantly, suggesting a faster decay of the continuum emission in the case of UV excitation compared to NIR excitation.

Aragon et al. [52] studied the evolution of line intensity and of line-to-continuum ratios and found that both depend on the specific spectral line and the laser pulse energy. They concluded that line intensities and line-to-continuum ratios cannot be simultaneously optimized for all elements using a single detection time window. Sabsabi and Cielo [53] investigated the temperature evolution in a nanosecond Nd:YAG-induced plasma on aluminum and copper targets in air. In both cases, they observed a similar temperature behavior, characterized by a rapid decrease during the first few microseconds (from approximately 1 eV to 0.5 eV) and smaller changes at later times on the microsecond scale. A similar trend over time was reported by Leis et al. [54], who determined the time-resolved temperature for a series of binary Fe–Cr alloys with iron content ranging from 10 to 100%. While the overall temperature evolution was similar for all the samples, the absolute temperature values differed by approximately 50%, with the pure iron sample exhibiting the highest temperature.

2.3 Ambient Gas

At elevated power densities, the efficiency of laser–material coupling is diminished due to the plasma shielding effect. The significance of plasma shielding is influenced by various factors, including the characteristics of the gas environment. Grant and Paul [55] conducted measurements of the spatially resolved emission intensity of a laser-induced plasma generated by an excimer XeCl laser on a steel target across different gaseous atmospheres (air, helium, and argon) and pressures (0.5, 50, and 760 torr) along the axial direction. Despite the limitations of a non-time-resolved apparatus, they observed a reduction in Laser-Induced Breakdown Spectroscopy (LIBS) signals for all types of ambient gases at a pressure of 0.5 torr. Furthermore, it was evident that signal-to-noise ratios decreased in close proximity to the target surface. The overall behavior of emission intensity concerning the three variables (gas, pressure, axial distance) proved to be too complex for a singular interpretation. Nonetheless, the study indicated optimal conditions for achieving the best signal-to-noise ratio, specifically in an argon atmosphere at a pressure of 50 torr, with the LIBS signal recorded approximately 6 mm from the target surface. Conversely, Leis et al. [54] proposed an argon ambient pressure of 140 torr to achieve higher intensity values, which were measured for the Si I 288.2 nm line in a steel sample using a Nd:YAG laser with a pulse energy of 5 mJ.

Sdorra and Niemax [56] compared the effect of different ambient gases (argon, neon, helium, nitrogen, air) on the production of plasma by means of a nanosecond Nd:YAG laser on a copper target. For fixed experimental conditions, and in particular at pressures lower than atmospheric, argon was demonstrated to produce the highest plasma temperature, the highest electron density, and, despite the lower mass ablation rate, the highest emission intensity for the chosen monitored element. Furthermore, the decay rate of the temperature during the first 40μs after the laser pulse was slower for argon than for the other gases. The same behavior was also found by Iida [57]. Helium, conversely, produced lower temperature, electron density, and emission intensity. In conclusion, argon was found to be most efficiently heated by inverse bremsstrahlung, generating buffer plasma that optically shields the target surface, thus reducing the amount of mass ablated. The shielding effect also occurs in the presence of other gases, but only for pulse energy values greater than 20mJ, while in argon there is a strong effect already at laser energies of approximately 10mJ. However, argon is found to yield the highest analyte emission intensity, except at high pressures, when neon offers the best performance. Again, similar results were shown by Iida [57], who measured the higher emission intensity with an argon atmosphere at approximately 100 torr pressure.

Kim et al. [58] observed the same signal increase and longer plasma lifetime in an argon atmosphere, as already described, and explained this phenomenon by the smaller conductivity and specific heat of argon gas compared to the corresponding air values. Such differences in thermal properties result not only in a higher temperature plasma leading to stronger emission but also in slower cooling of the plasma, leading to a longer emission period. Another important effect of the argon environment is the protection of the excited atoms from forming stable compounds such as oxides, which might reduce the LIBS emission from the analyte.

At low ambient pressure (< 1 mbar), the ablated vapor can expand almost freely, causing the outer part of the plasma to become colder than the core due to higher energy loss. When the pressure is increased to approximately 1 mbar, the confining effect of the ambient vapor reduces energy loss and results in a more uniform distribution. Hermann et al. [59] studied the time and spatial evolution of electron density and temperature by varying the laser power density and ambient pressure. Under their experimental conditions, they found that electron density was more sensitive to changes in power density than temperature. They also observed that the plasma lifetime—measured from line intensity as well as from the decay rate of Ne and T—increased with power density. This can be explained by the fact that plasma density increases with laser power density, making self-absorption of spectral lines more significant. Consequently, radiation loss is reduced, leading to an increased plasma lifetime. As the ambient pressure is increased from 0 to 1 mbar, the electron temperature and density remain unchanged during the early time frame (t < 200 ns after the laser pulse). However, decay rates for later times are reduced due to the confinement of the vapor plasma by the ambient gas, which prevents electrons or ions from rapidly escaping the observation point and facilitates the atomization of droplets and particles. Compared to free expansion in a vacuum, elastic and inelastic collisions occur between the target vapor and ambient gas species, resulting in a slower decrease in plasma density. Additionally, due to inelastic collisions, some kinetic energy is converted to excitation energy.

Thiem et al. [60] noted that analysis at atmospheric pressure is hindered by a broadband background emission spectrum generated by atmospheric elements. They preferred using a vacuum chamber to achieve better signal-to-noise ratios. In specific cases, certain arrangements must be made; for instance, if a UV spectrum down to 180 nm is to be observed, the experimental housing must be filled with nitrogen or another inert gas to prevent absorption of the LIBS signal by oxygen molecules.

3. Characterization of laser induced plasmas

The light emitted from laser-induced plasmas (LIP) serves as a valuable measure, providing both qualitative and quantitative information about the sample and the properties of the plasma itself [61]. The primary plasma properties that influence light emission are temperature, electron density, and the number densities of emitting species [62].

3.1 Calculation of LIPS Temperature

Knowledge of LIPS temperature is crucial for understanding the complex processes of dissociation, atomization, ionization, and excitation, as well as for enhancing the application of LIBS [63-66]. Additionally, understanding the gas temperature of the plasma is essential for various applications, including surface modification, material processing, thin film deposition, and the remediation of hazardous gases [67-68].

For a specific state of plasma, the excitation temperature can be determined from the intensity measurements of its spectral lines, assuming that the population of the energy levels follows the Boltzmann distribution law. This assumption requires that the plasma is in local thermodynamic equilibrium (LTE) or near LTE. The intensity of a line from level i to level j is given by:

$$I_{ij} = \frac{h\upsilon}{4\pi} L\, d\Omega\; g_i A_{ij} \frac{N_o}{U(T)} \exp\left\{-\frac{E_i}{kT}\right\} \quad (2)$$

L is the thickness of the plasma layer, h is Planck's constant, □□ =c/□□is the frequency, d□ is the solid angle, A_{ij} is the transition probability, N_o is the total density of atoms or ions, g_j is the statistical weight, U (T) is the partition function, E_i is the excitation energy of the upper level, k is Boltzmann constant, and T is the excitation temperature.

Before proceeding with temperature measurements of LIP, let us briefly discuss three important factors: LTE criteria, the selection of spectral lines, and verification methods for optical thin plasma.

LTE Criteria

The condition for complete LTE can be relaxed considerably since only the upper levels of the spectral lines used for the Boltzmann plots need to be in collisional equilibrium (Partial LTE). This can be estimated using the McWhirter criterion [69].

$$N_e \geq 1.6 \times 10^{12}\ T^{1/2}(\Delta E_{ij})^3 cm^{-3} \quad (3)$$

Where ΔE_{ij} is now the energy difference of the upper levels.

Moreover, before investigating how these factors influence LIP temperature, it is important to understand the origin of the term and the criteria for spectroscopic calculation. However, the term "temperature" is only valid when a certain fraction of the plasma meets the conditions of local thermodynamic equilibrium (LTE) [70].

(i) Selection of spectral line

Since the method of calculating the temperature is spectroscopic, the criteria for selection of spectroscopic lines concisely are [61]

(1) The lines must have reasonable line-to-background ratio.
(2) The spectral efficiency should be measured accurately.
(3) The greater the gap between the upper energy levels of selected lines (1-2 eV), the better the accuracy of the temperature measurement.
(4) The accuracy of spontaneous transition probability is relatively high.
(5) Special care should be taken to avoid lines affected by self-absorption, i.e. resonance lines or lines having low-lying energy levels.
(6) Their profiles should not influence by self-absorption.

(ii) Verification methods of optically thin lines

It is crucial to testify that plasma is optically thin for the spectral lines used for obtaining precise temperature results. Self-absorption relies on the line parameters involving degeneracy, oscillator strength, level energies, as well as plasma parameters such as temperature, electron density, and number densities of different species [71-72] The criteria for verification that the plasma is optically thin are concisely summarized herein [61]:

(1) For the multiple lines of a species whose lower/upper terms have a single level, the intensity ratio of them is in accordance with the statistical weight ratio [73-77].
(2) The intensity ratio of two atomic lines having the same upper level energy should be within the limit defined by a branching ratio [66, 70, 78-81], namely:

$$\frac{I_1}{I_2} = \frac{g_1 A_1 \lambda_2}{g_2 A_2 \lambda_1}$$

(3) The optical depth of the plasma should be much lower than 1, namely,

$$\kappa(\lambda_0) D(cm) \ll 1$$

Where $k(\lambda_o)$ is the absorption coefficient, D (cm) is the thickness of the plasma [82-85]. The absorption coefficient k $k(\lambda_o)$ (cm^{-1}) can be referred as [86]

$$\kappa_{ij}(\lambda_0) = 8.85 \times 10^{-13} f_{ij} \lambda_0^2 N_i P_{ji}(\lambda_0)$$

Where f_{ij} represents the oscillator strength; N_i (cm^{-3}) the number density of the lower energy level; P_{ji} (λ_0) the normalized line profile at the center of a Lorentzian profile line $P_{ji}(\lambda_0) = 1/(\pi\ \Delta\lambda_{1/2})$ in which $\Delta\lambda_{1/2}$ (cm) is the FWHM.

(4) The value of self-absorption coefficient defined as:

SA should be close to 1, where $\Delta\lambda$ stands for the experimental Stark width of the line; W_s for the half-width Stark broadening parameter, and $\alpha = -0.54$ [87-88].

(5) The curve of growth of the line should be a straight line [88-90].

Radziemski et al. [75] utilized the NI triplet at wavelengths 414.3 nm, 414.5 nm, and 415.1 nm to verify that the plasma was optically thin when the intensity ratio of these lines approached their statistical weight ratio of 1:2:3. Hegazy et al. [66, 70, 78-81] considered the spontaneous transition probability A and wavelength based on the statistical weight ratio g for the O I, Ti II, Mn I, and Cu I doublet spectral lines.

When the plasma is in Local Thermodynamic Equilibrium (LTE) or Partial Local Thermodynamic Equilibrium (PLTE), various approaches are employed by different research groups. These approaches are partly summarized by Hahn et al. [91] and comprehensively listed by S. Zhang et al. [61]. The methods include the Boltzmann two-lines method, the Boltzmann plot method, the Saha-Boltzmann two-lines method, the Saha-Boltzmann plot method, the line-to-continuum ratio method, and the synthetic spectra method [61, 91].

$$SA = \left(\frac{\Delta\lambda}{2w_S}\frac{1}{N_e}\right)^{1/\alpha}$$

In this review, we will discuss temperature calculations based on Boltzmann plots for plasmas produced from different target materials (Al, Ti, and Cu). We will consider the laser parameters that affect the performance of Laser-Induced Plasmas (LIPs) and the properties of the resulting plasma, such as laser energy and laser wavelength. Two different setup configurations were used for collecting the plasma emission [50, 66, 70, 78-81]. The first setup employed a quartz fiber cable to conduct the emitted light from the plasma plume to the entrance hole of an Echelle spectrograph. The fiber tip was positioned using an x-y translational stage [50, 79-81]. In the second setup, the plasma was imaged 1:1 by a quartz lens (f=20 cm) onto the entrance port of the Echelle spectrograph, as noted in references [66, 70, 78].

In this section, we will provide a brief review of our group's work on using spectral lines for temperature measurements, considering factors such as LTE criteria, the selection of suitable spectral lines, and the assessment of their optical thickness. H. Hegazy [79] tested three O I spectral lines at

wavelengths of 777.34 nm, 794.93 nm, and 848.65 nm, emitted from plasma produced by laser incidence on an aluminium target in an air atmosphere. These lines were evaluated for self-absorption based on their branching ratios, and the experimental ratios aligned with the optically thin limit calculated using these ratios.

H. Hegazy et al. [80] examined the effect of laser beam energy on the temperature of the plasma generated by focusing a Nd-YAG laser beam onto a solid aluminium target in an air atmosphere at the fundamental wavelength. The temperature evolution versus laser energy is illustrated in Figure 2.

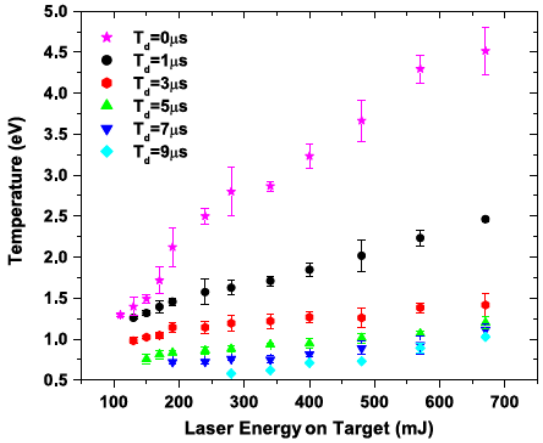

Figure (2): Temperature evolution vz the laser energy [80].

The same trend of the variation of the temperature with the laser energy incident on the target is also seen when the temperature of the plasma is calculated, which is generated by focusing an intense laser beam on a Zn target [50a,b] and a Cu [81] target in air at atmospheric pressure. The temperature is measured by developing a Boltzmann plot from Fe I spectral lines at 362.146, 363.146, 364.78, 371.99, 375.82, 376.38 and from Zn I spectral lines at 472.26, 481.08, 636.23nm, in case of the Zn target [50a,b], and from three Cu I spectral lines at 510.55, 515.32, 521.82 nm [81] in the case of the Cu target. Plasma are produced by two laser beams at the wavelengths (1064 and 532nm) at different laser energies. The spectral lines are tested to be free from self-absorption using the branching ratio. The resultant temperature variation versus the laser energy can be seen in Figure (3) and Figure (4) for the plasma produced from the Zn target and the Cu target, respectively.

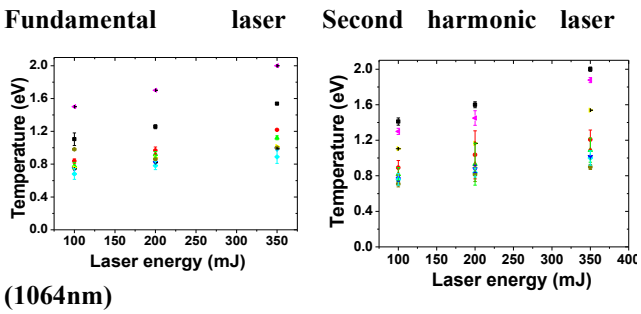

Figure (3): Temperature versus the laser energy incident on the Zn target [50a].

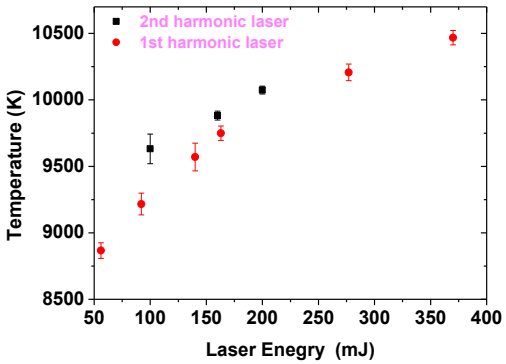

Figure (4): Temperature versus the laser energy on the Cu target [81].

The evolution of plasma produced by the interaction of pulsed laser beams (IR at 1064 nm and visible at 532 nm) with a titanium target in ambient air at atmospheric pressure was studied by H. Hegazy et al. [66]. Boltzmann plots were used to calculate the excitation temperature using Ti II spectral lines at 286.23, 321.71, 325.29, 348.36, and 351.08 nm. This set of lines was tested and confirmed to be suitable for measuring plasma temperature, as it was demonstrated that the lines were not affected by self-absorption using the previously stated branching ratio. The resulting temperature aligns well with that obtained from Ti II spectral lines suggested earlier by Hermann et al. [92]. This agreement is illustrated in Figure 5 for the plasma produced by both lasers.

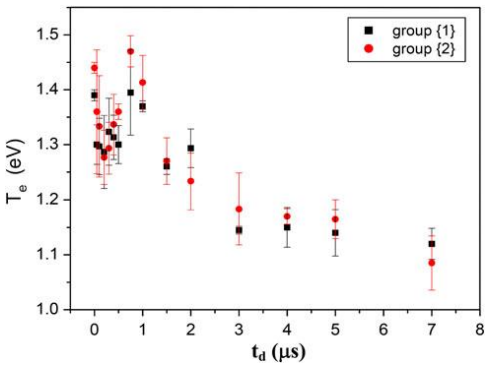

(a)

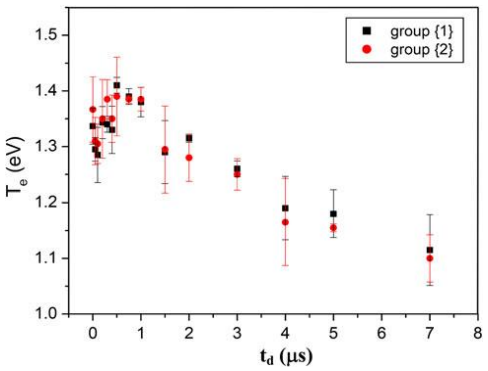

(b)

Figure (5): Temperature evolution of Ti plasma generated by (a) 1064 nm laser and (b) 532 nm laser [66].

The study of the emission spectrum of titanium plasma generated by lasers at wavelengths of 1064 and 532 nm, analyzed at various delay times under atmospheric pressure,

reveals that an intense continuum emission is produced instantaneously when the laser pulse reaches the target surface. This continuum emission decreases rapidly with increasing delay time. Generally, the spectra induced by the second harmonic laser exhibit a lower continuum contribution, shorter duration, and better resolution of the spectral lines compared to those produced by the fundamental laser wavelength. The present experiment demonstrates that the second harmonic laser-induced plasma (LIP) decays for a longer duration than the fundamental LIP, as the recombination process occurs more slowly. It is likely that the temperature is higher near the target surface, as the leading edge of the laser pulse quickly heats, melts, and vaporizes material just above the surface. Some of the laser energy subsequently heats the evaporated material. In an ambient gas, the expansion of the laser-produced plasma from the target material can be quite complex and is strongly influenced by various factors, such as atomic mass, background atoms, initial plume energy, and density. The dynamics of plume expansion are determined by the interaction of plasma species with the background gas, resulting in changes to the properties of the plasma emission.

The temperature derived from the Boltzmann plot represents the effective excitation temperature, which, by theoretical definition, equals the electron temperature. This implies a Maxwellian electron velocity distribution, contingent upon the existence of a Maxwell distribution and a Boltzmann distribution among the upper levels during the duration of the laser pulse. At time t = 0, a laser pulse lasting a few nanoseconds strikes the target, and since the ICCD gating duration is 2ms, the data are averaged over this 2 ms period at all subsequent times. The time required to establish a Maxwell distribution is dictated by the electron-electron collision time and the collision time for local thermodynamic equilibrium (LTE) between the upper levels. Estimates suggest that electron–electron collision times are less than 1ps at the initial high densities, thereby justifying the assumption of a Maxwell distribution and a corresponding temperature. At these electron densities, collisions among the upper levels also occur rapidly enough to establish partial LTE (PLTE) between high-lying levels, with respective times estimated to be less than the laser pulse duration of 1 ns.

In continuation of the titanium plasma studies, H. Hegazy et al. [78] measured variations in the plasma parameters of Ti plasma generated by 1064 nm and 532 nm lasers at different pressures in a nitrogen atmosphere for various delays. The temperature was calculated from the Boltzmann plot of five Ti II spectral lines, which we have previously validated for accuracy and stability in temperature measurements [66]. This work demonstrates that the intensities of Ti II spectral lines are significantly higher for plasma generated by the 1064 nm laser compared to those produced by the 532 nm laser across all pressures of ambient N_2 gas. It is noted that the higher intensity of spectral lines may be attributed to an increased ablation of the sample. The mass ablation of the metal depends on the thermodynamic and optical properties of the sample, as well as on the laser properties (wavelength, pulse duration, and irradiance). The ambient atmosphere (N_2) plays a crucial role in the mass ablation rate in conjunction with the properties of the incident laser beam. Consequently, changes in the properties of the plasma emission arise from alterations in plume expansion, which are determined by the interaction between the plasma and the ambient atmospheric atoms. The plasma temperature in this study was notably high during the initial stages but decreased rapidly over time while increasing with higher pressures of ambient N_2 gas, as illustrated in Figure 6.

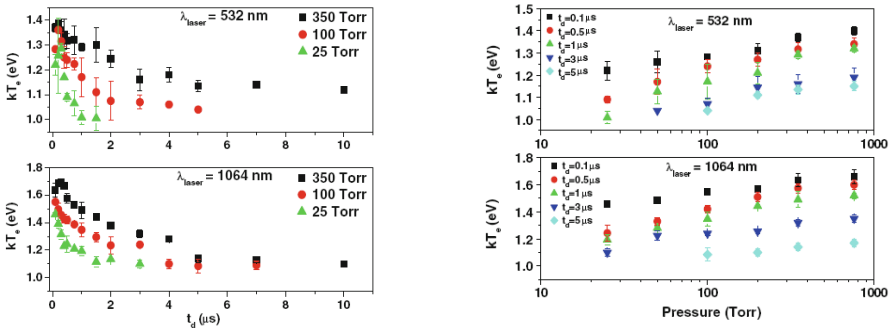

Figure (6): Temperature evolution of Ti plasma at different nitrogen pressure for both laser wavelength 1064 and 532 nm [78].

Mn I and O I spectral lines are utilized to evaluate the plasma generated for enhancing the capabilities of the laser-induced breakdown spectroscopy (LIBS) technique on aluminium targets [70]. The temperature of the resulting plasma has been determined using a Boltzmann plot of six Mn I spectral lines at 470.972 nm, 472.74 nm, 473.91 nm, 475.40 nm, 478.34 nm, and 482.35 nm, as introduced by Stavropoulos et al. [93], along with three O I lines at 777.34 nm, 794.93 nm, and 844.65 nm, as reported by H. Hegazy [79] for plasmas produced by lasers with wavelengths of 1064 nm and 532 nm. The spectral lines were tested and found to be free from self-absorption using the branching ratio method. The temperature evolution of the produced plasma is illustrated in Figure 7.

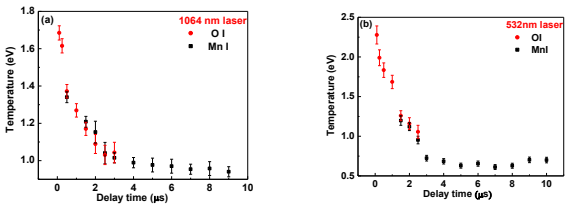

Figure (7): Temperature evolution for (a) 1064nm laser and (b) 532 nm laser [70].

The temperature evolution from various target materials, as measured by different thermometric elements, aligns well with the work of numerous authors, as extensively reviewed

by S. Zhang et al. [61]. As time progresses, the plasma temperature exhibits a decreasing trend due to several energy loss mechanisms, including thermal conduction to the background gas and target, cooling of the plasma through expansion against ambient pressure, and radiative cooling. In most cases, the plasma temperature decreases rapidly - sometimes exponentially- during the early stages of plasma expansion, remaining relatively constant until the end of spectral emission, as illustrated in Figure 8 [61].

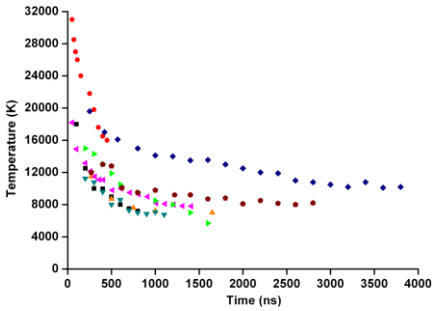

Figure (8): The decreasing trend of LIP temperature as time elapses [61]. The data sets are regenerated from various studies. ● (94), ◆ (95), ▶ (96), ⬟ (97), ◀ (98), ▼ (99), ▲ (100), ■ (101).

3.2 Calculation of LIP Electron Density

Stark broadening measurements of spectral lines are regarded as the most effective spectroscopic technique for determining the electron density in dense plasmas. This method assumes that the Stark effect is the dominant broadening mechanism, with Doppler broadening and pressure broadening due to collisions with neutral atoms (i.e., resonance and Van der Waals broadenings) being negligible. The validity of this assumption has generally been accepted in studies of laser-induced plasma and has been justified in various research works [85, 102-103]. For well-isolated lines in neutral and singly ionized atoms, Stark broadening is primarily driven by electron collisions. Since Stark broadening is only weakly dependent on temperature, the electron density can be determined with good accuracy.

The full width at half maximum (FWHM) of Stark-broadened lines is related to the electron number density [104-105] and can be expressed as follows:

$$\Delta\lambda_{1/2} = 2W\frac{N_e}{10^{16}}\left[1+1.75A\left(\frac{N_e}{10^{16}}\right)^{\frac{1}{4}}\left(1-\frac{3}{4}N_D^{-\frac{1}{3}}\right)\right] \quad (4)$$

Where, W is the electron impact parameter or Stark width parameter, N_e is the electron density in cm^{-3}, A is the ion impact parameter, and N_D is the number of particles in the Debye sphere which can be estimated from the relation

$$N_D = 1.72\times10^9\frac{T_e^{\frac{3}{2}}}{N_e^{\frac{1}{2}}} \quad (5)$$

W and A are functions of temperature and can be obtained approximated by second order polynomials from reference [105].

In laser-induced plasma where low temperature and high densities are present, the contribution of Doppler, Van der Waals, and resonance broadenings are very weak so the second term of the equation (4) can be neglected. Then,

$$\Delta\lambda_{1/2} = 2W\frac{N_e}{10^{16}} \quad (6)$$

Selection of the suitable spectral lines for the measurements of the electron density from the Stark FWHM in plasmas should meet certain requirements (see Wujec et. al. (106)) and the lines must not be affected by self-absorption.

Few spectral lines have a suitable Stark profile in the laser produced plasma emission in air; such as OI line at 844.65 nm [79-80], the Hα line at 656.27nm [70, 80, 107], the Al II spectral lines at 281.6 nm, and 466.3 nm [50, 70, 80], and the Si I line at 288.15 nm [50,70]. The Ti II spectral line is used for density measurements from a titanium produced plasma in air [66] and in nitrogen atmosphere [78].

Estimation of the absorption coefficient of Al II (281.6 and 466.3 nm) and Si I (288.15) lines based on the procedures described by Colon et al. [108] reveals a negligible value for the density range between 10^{17} and 10^{18} cm^{-3} [50, 70, 80]. For the Hα-line it had been proved previously that it is not affected by self-absorption [80, 107] for the same experimental conditions. However, the relative intensity of Hα and Hβ lines confirm the absence of self-absorption of the Hα-line, which can be attributed to the small concentration of the water vapor coming from the natural humidity of the ambient air. Doublet of O I [70, 79-80] spectral lines [I (777.34 nm) / I (844.65 nm)] is used for the assessment of self-absorption of the O I spectral line at 844.65 nm as mentioned in the temperature measurement section using the branching ratio method. Values of the Stark constant ($\alpha_{1/2}$) for Hα and the Stark constant and for non-hydrogenic lines are given in table (1).

Table (1): Stark constant and reference for Hα , OI, Al II, and Si I

Spectral line	Hα 656.27 nm [109-110]	O I 844.65 nm [109]	Al II 281.65 nm [108,111]	Al II 466.30 nm [108]	Si I 288.15 nm [111]
Stark constant (nm)	0.021	1.236	0.00212	0.00603	0.095
N_e^{ref}	8.02×10^{12}	10^{18}	10^{16}	10^{16}	5.6×10^{17}

These spectral lines exhibited approximately Voigt line shapes. The analysis of the line profile was conducted as follows: the measured instrumental profile was convoluted with a Lorentzian profile representing the Stark profile of variable width using a Matlab. Subsequently, the resultant Voigt profile was compared to the measured spectral line

through the least squares fitting method, iterating a certain number of times until a good agreement was achieved. This process yields an accurate value for the Stark full width at half maximum (FWHM) of the spectral line of interest. The measured instrumental width is determined by calculating the FWHM of the Hg lines emitted by a standard low-pressure Hg lamp. These lines are utilized to study density evolution at different laser energies, as referenced in (68) and illustrated in Figure (9).

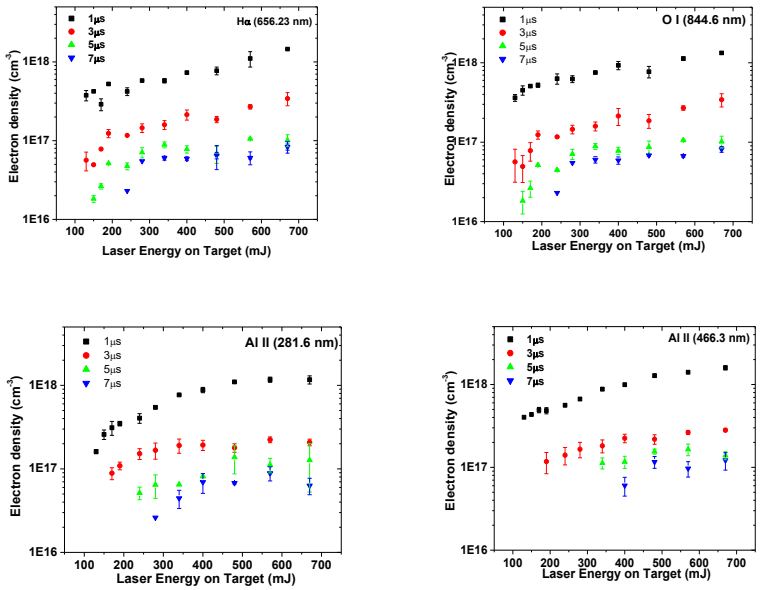

Figure (9): Density evolution of Al plasma produced by 1064 nm laser using H□, OI, Al II [80].

These lines in addition to the Si I line at 288.15 nm are used for the evaluation of the plasma produced for enhancing the capability of laser induced breakdown spectroscopy (LIBS) technique for plasmas produced from Al targets [70]. In this work, the temporal evolution of the electron density of the plasma produced by the two laser wavelengths 1064 and 532 nm are presented in Figure (10).

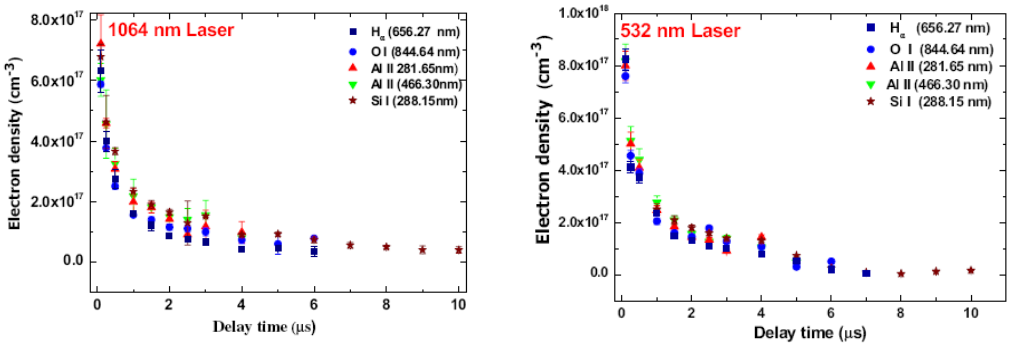

Figure (10): Density evolution of Al plasma produced by the laser wavelength 1064 nm and 532 nm [70].

The Ti II spectral line is used for density measurements from a titanium produced plasma in air [66] and in nitrogen atmosphere [78]. In these studies the density evolution in air and in nitrogen atmosphere is studied for both laser wavelengths 1064 and 532 nm. Figure (10) present the evolution at different nitrogen pressure as an example [78].

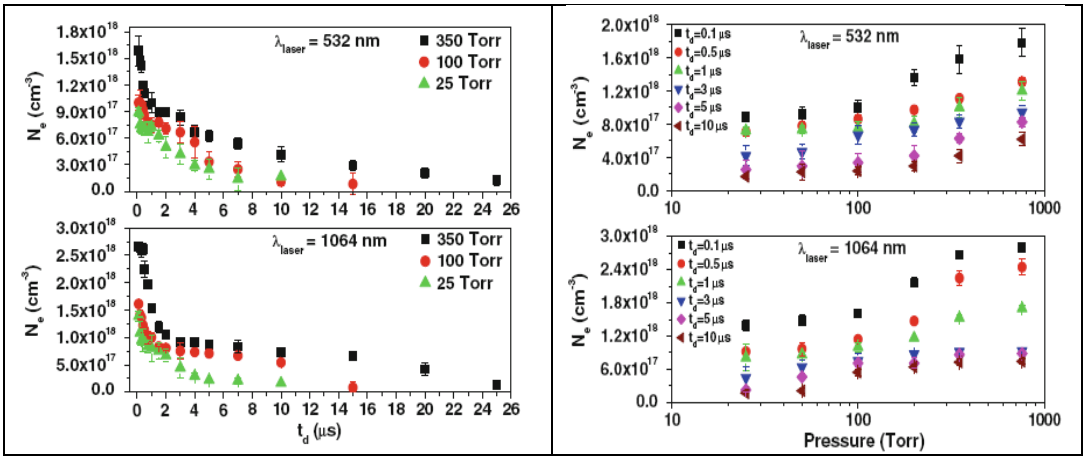

Figure (10): Density evolution of Ti plasma at different nitrogen pressure for both laser wavelength 1064 and 532nm [78].

4. Laser produced plasma applications

4.1 Laser Induced Breakdown Spectroscopy (LIBS) for Elemental Analysis

LIBS is becoming a dominant technology for direct solid sampling in analytical chemistry. LIBS refers to the process in which an intense burst of energy delivered by a short laser pulse is used to sample (remove a portion of) a material. The advantages of LIBS in elemental analysis include direct characterization of solids, no chemical procedures for dissolution, reduced risk of contamination or sample loss, analysis of very small samples not separable for solution analysis, and determination of spatial distributions of elemental composition. LIBS as mentioned above can be regarded as a universal sampling, atomization, excitation and ionization source since laser induced plasmas can be produced in gases [112] or aerosols [75, 112-113] or liquids [21, 114-117], and as well as from conducting or non-conducting solid samples [118-121]. Moreover, LIBS offers on-line measurements in industries with the compact new technologies of spectrometers with ICCD cameras [112,117, 51, 122-125]. In the strictest sense, LIBS cannot be considered a non-destructive technique since part of the target to be analyzed is vaporized and lost. However, the volumes sampled in this manner are very small. It ranges from 10^{-8} – 10^{-5} cm^3 depending on the material's base, the laser wavelength, and the fluence which corresponds to the masses in the ng–µg range. Moreover, sample vaporization and excitation is possible in a single step i.e. there is no need for particles to be transferred to an external source [73].

LIBS measurements involve spectral and time-resolved analysis of the atomic and ionic emission lines generated at the surface of a sample by a focused, intense laser pulse [126-128]. Since the early applications of LIBS for diagnostic purposes, various systems have been developed for both laboratory and portable use [129-131]. In the LIBS technique, the extremely high field intensity instantly evaporates a thin surface layer and initiates avalanche ionization of the sample elements, resulting in the breakdown effect. LIBS spectra can be detected once the plasma's continuum emission nearly extinguishes. Time-resolved capability is essential for distinguishing late atomic line emissions from early plasma continuum emissions. High-resolution spectral analysis is necessary to detect individual emission lines, which represent the spectral signatures of each element. The atomic and, in some cases, ionic lines, once attributed to specific transitions, enable qualitative identification of the species present in the plasma. Their relative intensities can be utilized for the quantitative determination of the corresponding elements. This method can be validated for analytical applications in material analysis within industry, provided that the surface composition is maintained in the plasma and that the ablation process can be modelled within an appropriate temporal window under quasi-equilibrium conditions. Other studies [130, 132] have shown that various experimental parameters (e.g., laser power, repetition rate, interaction geometry, surface conditions) can influence the method's effective analytical capabilities, particularly in field applications that could leverage its main advantage of requiring no sample pre-treatment.

The main parameters affecting the performance of Laser-Induced Breakdown Spectroscopy (LIBS) include laser intensity, excitation wavelength, laser pulse duration, and the physical and chemical characteristics of the target material, as well as its surface conditions, particularly the surrounding atmosphere [117]. While numerous studies have investigated the parameters influencing plasma characteristics, there is relatively limited knowledge about the impact of laser pulse duration on LIBS calibration curves [133-134]. For accurate quantitative analysis, it is crucial to avoid self-absorption, spectral overlap (including spectral line interference and band interference), and matrix effects (chemical interferences) in LIBS [135]. The physical and chemical properties of a sample can affect plasma composition, a phenomenon known as the matrix effect, which can lead to differences in ablation between the sample and the target material. Several researchers have studied the matrix effect under various experimental conditions to identify its causes and develop correction methods [118-119, 134-137].

Despite its advantages and recent success, LIBS has lower sensitivity than some traditional analytical techniques such as atomic emission spectrometry of inductively-coupled plasma (ICP-AES) and laser ablation inductively coupled plasma mass spectroscopy (LA-ICP-MS) [138].

Double pulse (DP) LIBS introduced for the improvement of the sensitivity and limit of detection (LOD) of the LIBS [139-141]; however, detection limits improved by orders of

magnitude compared to conventional single pulse (SP) LIBS. DP refers to two pulsed lasers separated in time by ns or even μs delays. The beam arrangements commonly used are collinear and orthogonal. Possible explanations for the higher intensity observed include an increase of the ablation efficiency due to lower laser shielding, heating of the target surface and its vicinity and confinement of the second plume in a low density zone generated by the first shock wave [142]. However, the physical mechanisms involved are still not clearly understood.

Ciucci, et. al. [125] in 1999 introduces the calibration-free LIBS as a new procedure for quantitative elemental analyses of the materials. The method presented, based on an algorithm developed and patented by IFAM-CNR, allows the matrix effects to be overcome, yielding precise and accurate quantitative results on elemental composition of materials without use of calibration curves. The approach of multi-elemental quantitative analysis of LIBS spectra, based on the measurement of line intensities and plasma properties (plasma electron density and temperature) and on the assumption of a Boltzmann population of excited levels, which does not require the use of calibration curves or matrix-matched standards[170].

Advances in the SP-LIBS measurements using a certified samples of known concentration for building a calibration curves were achieved by studying the accumulation of consecutively measured emission spectrum of the Al plasma produced by 10, 20, 50, and 100 laser pulse and accumulate it on ICCD camera using a Nd-YAG laser at the fundamental wavelength (1064nm) [143] and using second harmonic laser (532nm) [144]. However, compromising the obtained results of SNR and self-absorption at different delay times, it is found that 50 of accumulated consecutively measured spectra on ICCD reveal a high SNR and play a role in reducing the effectiveness of self-absorption of different spectral lines tested for the elemental composition of the test sample. LOD and the precision at different laser pulse energy compared with other results by different authors [73, 119,111, 145-151] are shown in table (2). Improvements of the determined LOD for the fundamental wavelength are obtained for Cu I at 521.85 nm, Si I at 288.15 nm, Mn I at 482.34 nm, and Cr I 520.84 nm spectral lines and are shown in table (3) in comparison with other works [146, 148-149]. The LOD is 83.8% for Cu I line at 521.85 nm, 49% for Si I at line 288.15 nm, 84.3% for Mn I line at 482.34 nm, 45% for Cr I at line 520.84 nm lower than the previous reported works.

Table (2): Limit of detection (LOD) for the elements [143] in comparison with other works from different labs and energies E=70mJ [119], E= 60mJ [73, 145 and 151], E=50mJ [147], E=300mJ [148], E=65mJ [111], E=15mJ [149], E=90mJ [149], E=30mJ [150].

Element	λ (nm)	RSD %	LOD (ppm)									
			[143]			Other works						
			23 mJ	220 mJ	440 mJ							
Cu I	324.72	18.79	48	44	17	23.8[119]	17.49[148]	33[111]	15[149]	150[146]	80[151]	---
	327.39	23.91	60	54.9	13	10[73]	---	---	---	---	---	---
	510.55	22.90	---	58.7	51.7	---	---	---	---	---	---	---
	515.36	26.60	---	43.6	42.1	---	---	---	---	---	---	---
	521.85	20.20	---	36.9	25.9	205[111]	160[149]	---	---	---	---	---
Mg I	517.26	23.70	170	73	36	0.5[73]	---	---	---	---	---	---
	518.36	22.50	94	39	25	3.19[148]	0.5[145]	---	---	---	---	---
Si I	288.15	20.17	90.8	70	35	283[119]	80[147]	68.74[148]	90[111]	2200[150]	100[146]	527[151]
Cr I	520.84	17.06	---	81	55	---	---	---	---	---	100[146]	---
Fe I	344.06	21.738	---	55.3	53.7	----	---	----	---	---	---	---
	375.82	8.0953	---	259	219	---	----	---	---	---	---	---
Mn I	478.35	25.51	---	68	50.7	---	---	---	---	---	---	---
	482.34	20.80	---	65	47	300[146]	---	---	---	---	---	---

Table (3): LOD for the improved spectral lines and the improvements in percent [143].

Element	λ (nm)	LOD for previous works	LOD Present Work	Improvement Percent
Cu I	521.85	160 [149]	25.9	83.8%
Si I	288.15	68.74 [148]	35	49.08%
Mn I	482.34	300 [146]	47	84.3%
Cr I	520.84	100 [146]	55	45%

In case of plasma produced by the second harmonic laser at 532 nm [144], better improvements are achieved in comparison to plasma produced by the fundamental laser at 1064nm [143]. LOD and improvement percentages resulted are shown in table (4, 5).

Table (4): The LOD in ppm for LIBS by fundamental laser [143] and second harmonic laser [144] and the improvement in percent for low laser energy.

Element	λ (nm)	LOD for 1064nm 23 mJ [143]	LOD for 532nm 20 mJ [144]	Improvement percent
Cu I	324.72	48	19	60.4%
	327.39	73	20	72.6%
Mg I	517.26	170	43	74.7%
	518.36	94	33	64.8%
Si I	288.15	90.8	90	0.88%

Table (5): The LOD in ppm for LIBS by fundamental laser [143] and second harmonic laser [144] and the improvement in percent for the higher laser energy.

Element	λ (nm)	LOD for 1064nm 220mJ [143]	LOD for 532nm 188mJ [144]	Improvement percent
Cu I	324.72	44	13	70.4%
	327.39	54.9	18	67.2%
	510.55	58.7	22.5	61.6%
	515.36	43.6	56.9	----
	521.85	36.9	21.8	40.9%
Mg I	517.26	73	8.2	88.7%
	518.36	39	7.4	81. %
Si I	288.15	70	76	----
Cr I	520.84	81	11.6	85.6%
Fe I	344.06	55.3	23.8	57%
	375.82	259	29.6	88.5%
Mn I	478.35	68	57	16.1%
	482.34	65	52	20%

The emission intensities of the spectral lines produced by the 532 nm laser are significantly higher than those induced by the 1064 nm laser. This increased intensity may be attributed to greater sample ablation with the 532 nm laser. Consequently, the mass ablation with the 532 nm laser is greater than that with the 1064 nm laser for plasma generated in ambient air. This observation aligns with the findings of L. Fornarini et al. [152], which indicate that the mass ablation of metals depends on the thermodynamic and optical properties of the sample, as well as the laser characteristics (wavelength, pulse duration, and irradiance). Evaluations of plasmas produced by first and second harmonic nanosecond lasers under the improved conditions mentioned above have been conducted (see refs. 70, 153). The plasma temperature ranged from 0.73 eV to approximately 1 eV for different laser energies across both wavelengths, corresponding to the optimized plasma used for LIBS analysis [70, 153]. This temperature is very close to those commonly observed in other spectrochemical analytical techniques and excitation sources, such as Inductively Coupled Plasma – Optical Emission Spectrometry (ICP-OES) [154-155]. Furthermore, the determined density [70, 153] confirms that the plasma produced in the LIBS experiments operates in the LTE regime.

4.2 Applications of Laser Produced Plasmas in Tokamak Research

Laser ablation of solids using high-intensity nanosecond or femtosecond pulses results in complex interactions between the laser beam, the solid material, and the ablated material. Several processing parameters influence the dynamics of ablation and the properties of the generated plasma [156-158]. Some fundamental physical features, such as the nature of laser absorption in vaporized material and the acceleration mechanisms for ions, are not yet fully understood.

Plasma dynamics can be effectively controlled by applying a magnetic field in various ways. This is particularly relevant in inertial confinement fusion systems, where the magnetic field can potentially slow high-energy particles before they implant in surrounding structures. The presence of a magnetic field during the expansion of laser-induced plasma may initiate several interesting physical phenomena, including the conversion of plasma thermal energy into kinetic energy, plume confinement, plume splitting, ion acceleration, emission enhancement, and plasma instabilities. Many research groups are already involved in this area. It has been observed that most studies focus on plasma expansion in a uniform, constant applied field rather than in varying magnetic fields. To gain a better understanding, Sony George [159] conducted research using magnetic fields ranging from 0G to 4000G. Due to their relevance in tokamaks, Sony George [7, 159-162] also studied plasmas from lithium solid targets and laser blow-off plasmas from LiF-C thin film targets.

In laser-produced plasma (LPP), high-power lasers focused on solid materials, referred to as 'targets,' induce rapid ionization, causing the generated plasma to propagate in the opposite direction to the laser beam, perpendicular to the target surface. In contrast, the laser-induced forward transfer technique, also known as laser blow-off (LBO), involves the laser pulse interacting with a thin-film target, resulting in the plume propagating in the forward direction, aligned with the

laser beam. The LBO scheme consists of a laser and a substrate that is transparent to the laser wavelength [163]. The substrate is pre-coated with a layer containing the material to be injected, which must absorb the laser beam. This coating can consist of either a single species or a multilayer of several thousand angstroms in thickness. In this case, the ablated material propagates along the direction of the incident laser beam.

Edge plasma parameters in fusion machines are important as they play a key role in determining the global plasma confinement. Understanding and controlling the edge plasma parameters are important for designing the divertor in fusion reactors. Neutral atomic beams are well suited for the diagnostics of the tokamak edge plasma [163,164]. In LBO [7,159-162], short bursts of high intensity neutral atomic and ionic beams with energy 1–10 eV are generated. The super-thermal atomic beam is normally injected in a direction transverse to the toroidal magnetic field of the tokamak. Therefore, the study of the effect of the magnetic field on the production of atomic beam is of significant importance. The enhancement of spectral line emission from the ionic and neutral species, in the presence of transverse magnetic field, has been reported by several authors [164], in case of conventional laser produced plasma (LPP) experiments. This is attributed to an increase of the confinement of the plume and recombination processes. The plasma plume of (Li) consists of mainly neutral and singly ionized atoms [163], and hence recombination processes could lead to the enhancement of neutral emission lines. Therefore, it is interesting to see the behavior of LBO generated species (especially neutral species) in the presence of transverse magnetic field. As the study by Ajai Kumar et al. [7] reveals this is important from the point view of plasma diagnostic in tokamaks, since the value of the magnetic field depends on the location of the LBO system at the tokomak.

The spectrum of Li-like iron, Fe^{23+}, appears prominently in many types of high-temperature plasmas, such as they are found in tokamaks, laser-produced plasmas, and in the solar corona [5]. The spectrum is thus of great interest as a diagnostic tool for understanding these plasmas. Shirai et. al. [164] and Kim et. al. [166] calculated wavelengths of the 2s-2p resonance transitions for all Li-like ions from Z = 6 to Z = 92 with a Dirac-Fock code and compared their results with experiment and with other calculations. J. Reader et al. [5] observed the spectrum of Fe^{23+} with laser-produced plasma and with the plasma of a tokamak. In the spectra from the laser-produced plasma new lines of Fe^{23+} were observed that were identified as 3s-4p, 3p-4d, and 3d-4f transitions. The measured wavelengths of these lines were combined with measurements of the 2s-2p resonance lines measured in the tokamak plasma and with earlier measurements of n = 2 to n = 3 transitions to yield an improved system of energy levels for Fe^{23+}. With the 4f energy levels improved ionization energy for this ion was determined.

In high-temperature plasmas of tokamaks and fusion machines, electron temperatures are determined using the ratio of satellite line intensities relative to the resonance line. To ensure precise diagnostics, atomic data, including wavelengths, radiative transition rates, and autoionization rates, must be accurately known. N. Yamamoto et al. [6] developed a new method to infer plasma temperature and density using only satellite lines, as Ly-α lines are easily affected by opacity. They calculated atomic data for the satellite lines of H-like Mg using four different codes and compared all four data sets. By analyzing spectra observed from a laser-produced plasma with a high-resolution spectrometer, N. Yamamoto et al. [6] derived the electron temperature and density, comparing the observed spectra with theoretical spectra calculated using the different atomic data sets. The calculated atomic data proved very useful for measuring electron temperature and density in tokamak plasmas. However, due to the high plasma temperature, the hydrogenic components of the plasma and low-Z impurities are ionized up to bare nuclei. Intermediate-Z elements are ionized to He-like and H-like ions and exhibit strong emission lines in the X-ray spectral range. The precise modelling of He-like spectra from highly charged ions (Ar, Ti, and Fe) enables accurate measurements of tokamak plasma parameters. O. Marchuk [167] designed a theoretical simulation of the spectra, incorporating physical parameters of the He-like system, for fusion devices and solar flares in the low-density limit. Marchuk [167] successfully obtained the electron and ion temperatures and concentrations of highly ionized ions using the X-ray spectrometer installed at the TEXTOR tokamak. The developed model for He-like argon has also been applied to measurements of other elements on the TORE SUPRA tokamak. For accurate modelling, the most precise experimental values for wavelengths and other necessary atomic data (transition probabilities, cross sections, etc.) were obtained from measurements on electron beam ion traps (EBITs) and laser-produced plasma sources.

Fusion energy has great potential over other sources of energies due to the abundance of fusion fuel on the Earth and tokamak has turns out to be the best technique to harvest fusion energy. However, a continuous operation of a tokamak involves challenges due to plasma-wall interaction, e.g. erosion, re-deposition, fuel retention, and impurities control. For an efficient operation, the tokamak wall has to be remotely monitored. The diagnosis of the fuel retention and impurity deposition on the plasma facing components is very important for monitoring plasma-wall interactions and improving the performance of long-pulse operation for tokamak devices. D. Zhao et al. [168], developed a remote in situ laser induced breakdown spectroscopy (RIS-LIBS) approach for diagnosis of the plasma facing components (PFCs) on experimental advanced superconducting tokamak (EAST). For the test of detectable elements, the fuel (deuterium) and impurities have been detected and identified clearly. In addition, the measurement of fuel abundance on the first wall as a function of the days of EAST deuterium plasma discharges has been carried out for the first time [168]. The results well manifest a significant prospect of the RIS-LIBS for the diagnosis of the PFCs in the upcoming fusion devices like CFETR and ITER.

LIBS seems to be the most suitable technique for this purpose. Multiple LIBS techniques (e.g. back-collection, VUV LIBS, DP-LIBS) are reviewed by G. S. Maurya et al. [169]. In this contribution the role of pressure, excitation wavelength and atmospheric effect had also been discussed. LIBS studies of spatial and depth profiles of W, Be, Al, Mo, Li, C based materials with impurities are presented as well

and compared to other analytical methods. At last, the measurement of layer-wise matrix hardness is also discussed.

5. Conclusion

Unfortunately, many of the fundamental physical features involved in LIBS, such as the nature of laser absorption in the vaporized material, ion acceleration mechanisms, plasma homogeneity, shock wave propagation into the ambient atmosphere, and the plasma shielding effect, are still not fully understood. Plasma homogeneity is a particularly complex issue in LIBS experiments, as it depends on the spatial and temporal gradients of temperature and the number densities of both electrons and heavy species in the plasma. Due to its fast dynamics and interaction with the background environment, plasma inhomogeneities significantly affect LIBS performance. The peripheral zones of the plasma are particularly involved in processes such as recombination (between ions and electrons within the plasma or between species from the surrounding atmosphere and the plasma), as well as confinement effects by the shock wave contact wall. Consequently, differences may arise between plasma parameters in the outer regions and those in the plasma core. For diagnostic or analytical purposes, only the portion originating from the plasma core is typically used. In this context, the homogeneity assumption is considered valid, as demonstrated by several authors using spatially resolved LIBS spectra (see [170]). The validity of this assumption can be further ensured through appropriate experimental strategies, including the selection of temporal and spatial regions suitable for spectral acquisition, as well as data processing techniques for spatial resolution. In our own group's work [143,144], this issue is addressed by aligning the optical detection setup to image the plasma two millimeters from the target surface, which is positioned using an x–y stage with 100 µm resolution, and a He–Ne laser is used for alignment. To better understand the spatial distribution of plasma components, W. Wie et al. [171] reported that N II emission extended over a much broader region above the target surface compared to emissions from target elements in the early stages of plasma evolution. This observation provides evidence that laser-ablated plasmas were effectively confined by the ambient air, highlighting the role of confinement effects. Within tens of nanoseconds after the termination of the laser pulse, continuum radiation became negligible, and characteristic spectral lines began to dominate the emission spectrum. The spatial distribution of nitrogen remained broader than that of target-derived species. This broader presence of N II in the early stages may be attributed to ionization of ambient air via the shock wave, rather than through direct laser-target interaction. Although the nitrogen atoms possess high ionization energy, they may be pre-excited, and ionization could occur as the laser beam propagates through the ambient air. The shock wave, which propagates rapidly into the surrounding atmosphere, produces high pressure and temperature at its front, resulting in localized air ionization [172]. This mechanism also supports the observations made by S. S. Harilal et. al. [173], who found that the plasma emission front aligned closely with the shock wave front within the first 400 ns. Additionally, the partial ionization near the shock front was proposed to contribute to the acceleration of plasma flow [174]. It is important to note that both pressure and temperature near the shock front decrease steadily as the wave expands into the ambient air, and eventually becoming too low to sustain excitation or ionization of surrounding gas molecules

N. Farid et. al. [175] found the plasma shielding depends on the background ambient gas pressures which also change significantly the ablation, line and background emission. However, the shielding becomes dominant at higher pressures which is not only reducing the mass ablation but also absorbs the energy from the incidence laser resulting into higher temperature plasma in the front of the target surface.

With these challenges, the LIBS community will continue to work towards a better understanding of the important factors affecting the produced plasma in LIBS experiments. Recently, V. Palleschi et al. [176] published a comprehensive review guide to LIBS measurements, outlining crucial steps for optimizing experimental parameters, obtaining and analyzing high-quality spectra, and effectively reporting results. The review also examines the most promising existing applications and explores future directions that could establish LIBS as a viable alternative to conventional analytical methods.

Acknowledgment

Sincere thanks to Prof. N. Can Dept. of Physical Sciences, College of Science, Jazan University, Saudi Arabia for valuable discussions and revising this manuscript.

References

[1] C. Aragón and J.A. Aguilera, Spectrochimica Acta Part B 63 (2008) 893-916.
[2] S. Amoruso, R. Bruzzese, N. Spinelli and R. Velotta, J. Phys. B: At. Mol. Opt. Phys. 32 (1999) R131-R172.
[3] A. De Giacomo, V.A. Shakhatov and O. De Pascale, Spectrochimica Acta Part B 56 (2001) 753-776.
[4] A. De Giacomo, V.A. Shakhatov, G.S. Senesi and F. Prudenzano, Appl. Surf. Sci. 186 (2002) 533–537.
[5] J. Reader, J. Sugar, and N. Acquista, "Laser-produced and tokamak spectra of lithiumlike iron Fe23 + ", J. Opt. Soc. Am. B11 (1994) 1930-1934.
[6] N. Yamamoto, T. Kato and F. B. Rosmej, "Satellite Line Spectra of H-Like Mg Ions for Plasma Diagnostics and Atomic Data", J. Plasma Fusion Res. SERIES 7 (2006) 131-134.
[7] Ajai Kumar, Vishnu Chaudhari, Kiran Patel, Sony George, S. Sunil, R. K. Singh, and Ranjeet Singh, "An experimental setup to study the expansion dynamics of laser blow-off plasma plume in variable transverse magnetic field", Rev. Sci. Instrum. 80 (2009) 033503.
[8] Pulsed Laser Deposition of Thin Films, edited by D. G. Chrisey and G. K. Hubler, Wiley, New York, 1994.
[9] D. Bauerle, Laser Processing and Chemistry, 2nd ed., Springer, New York, 1996.
[10] M. von Allmen and A. Blatter, Laser–Beam Interactions with Materials, 2nd ed., Springer, New York, 1995.
[11] E. D'Anna, G. Leggieri, A. Luches, M. Martino, A. Perrone, G. Majni, P. Mengucci, R. Alexandrescu, I.

N. Mihailescu, and J. Zemek, Appl. Surf. Sci. 86 (1995) 170.
[12] I. N. Mihailescu, N. Chitica, E. Gyorgy, V. S. Teodorescu, G. Marin, A. Luches, A. Perrone, M. Martino, and J. Neamtu, J. Mater. Sci. 31 (1996) 2909.
[13] N. Chtica, E. Gyorgy, Adriana Lita, G. Marin, I. N. Mihailescu, D. Pantelica,M. Petrascu, A. Hatziapostolou, C. Grivas, N. Broll, A. Cornet, C.Mirica, and A. Andrei, Thin Solid Films 301 (1997) 71.
[14] S. Eliezer, N. Eliaz, E. Grossman, D. Fisher, I. Gouzman, Z. Henis, S. Pecker, Y. Horovitz, M. Fraenkel, S. Maman and Y. Lereah, Phys. Rev. B 69 (2004) 144119.
[15] S. Amoruso, G. Ausanio, R. Bruzzese, M. Vitiello and X.Wang, Phys. Rev. B 71 (2005) 033406.
[16] D. Scuderi, O. Albert, D. Moreau, P.P. Pronko and J. Etchepare, Appl. Phys. Lett. 86 (2005) 071502.
[17] A.L. Timur, M.P. Andrey, N.L. Vasily and B.Z. Nikita, Spectrochimica Acta Part B 64 (2009) 938–949.
[18] J. Ben Ahmed and N. Jaidane, Spectrochimica Acta Part B 64 (2009) 442–447.
[19] M. Khaleeq-ur-Rahman, K. Siraj, M.S. Rafique, K.A. Bhatti, A. Latif, H. Jamil, M. Basit, Nucl. Instrum. Meth. Phys. Res. B 267 (2009) 1085–1088.
[20] D.A. Rusak, B.C. Castle, B.W. Smith and J.D. Winefordner, Crit. Rev. Anal. Chem. 27 (1997) 257.
[21] L.J. Radziemski, D.A. Cremers, Laser induced plasma and applications, Marcel Dekker, New York, (1989).
[22] V. N. Raia and S. N. Thakurb, Physics of Plasma in Laser-Induced Breakdown Spectroscopy, in: Jagdish P. Singh, Surya N. Thakur, Laser-Induced Breakdown Spectroscopy, Elsevier press, Amestrdam (2007).
[23] J.M. Vadillo and J.J. Laserna, Spectrochimica Acta Part B 59 (2004) 147-161.
[24] R.E. Russo, X. Oleg, V. Borisov and H. Liu, Laser ablation in atomic spectrometry, Encyclopedia of Analytical Chemistry: Instrumentation and Applications, Wiley, Chichester, 2000.
[25] L. Moenke-Blankenburg, Laser Microanalysis, Wiley, New York (1989).
[26] L.M. Cabalin and J.J. Laserna, , Spectrochim. Acta Part B 53 (1998) 723-730.
[27] A. Vertes, R.W. Dreyfus and D.E. Platt, IBM J. Res. Dev. 38 (1994) 3-10.
[28] B.N. Chichkov, C. Momma, S. Nolte, F. Von Alvensleben and A. Tunnermann, Appl. Phys. A 63 (1996),109–115.
[29] X. Mao, W. Chan and R.E. Russo, Appl. Spectrosc. 51 (1997) 1047-1054.
[30] B. Le Drogoff, J. Margot, M. Chaker, M. Sabsabi, O. Barthe- lemy, T.W. Johnston, S. Laville, F. Vidal and Y. von Kaenel, Spectrochim. Acta Part B 56 (2000) 987–1002.
[31] V. Margetic, K. Niemaxb and R. Hergenroder, Spectrochim. Acta Part B 56 (2000) 1003–1010.
[32] R.E. Russo, X. Mao, J.J. Gonzalez and S.S. Mao, J. Anal. Atom. Spectrom. 17 (2002) 1072–1075.
[33] V. Margetic, M. Bolshov, A. Stockhaus, K. Niemax and R. Hergenroder, J. Anal. Atom. Spectrom. 16 (2001) 616–621.
[34] K.L. Eland, D.N. Stratis, D.M. Gold, S.R. Goode and S.M. Angel, Applied Spectroscopy 55 (2001) 286–291.
[35] S. Amoruso, M. Armenante, V. Berardi, R. Bruzzese and N. Spinelli, Appl. Phys. A 65 (1997) 265–271.
[36] G.M. Weyl, Physics of laser-induced breakdown: an update, in: L.J. Radziemski and D.A. Cremers (Eds.), Laser-Induced Plasmas and Applications, Marcel Dekker, New York (1989).
[37] W. Sdorra, J. Brust and K. Niemax, Microchim. Acta 108 (1992) 1-10.
[38] L.M. Berman and P.J. Wolf, Appl. Spectrosc. 52 (1998) 438-443.
[39] C.W. Ng, W.F. Ho and N.H. Cheung, Appl. Spectrosc. 51 (1997) 976–983.
[40] L.M. Cabalin and J.J. Laserna, Spectrochim. Acta Part B 53 (1998) 723-730.
[41] C. Haisch, J. Liermann, U. Panne and R. Niessner, Anal. Chim. Acta 346 (1997)23–35.
[42] E.H. Piepmeier and H.V. Malmstadt, Anal. Chem. 41 (1969) 700–707.
[43] G. Dimitrov and T. Zheleva, Spectrochim. ActaPart B 39 (1984) 1209-1219.
[44] M.A. Shannon, X.L. Mao and R.E. Russo, Mater. Sci. Eng. B 45 (1997) 172–179.
[45] X.L. Mao and R.E. Russo, Appl. Phys. A 64 (1997) 1–6.
[46] J.A. Aguilera, C. Aragon and F. Penalba, Appl. Surf. Sci. 127–129 (1998) 309–314.
[47] J.M. Vadillo, J.M. Fernandez-Romero, C. Rodrıguez and J.J. Laserna, Surf. Interface Anal. 27 (1999)1009–1015.
[48] R. Noll, R. Sattmann and V. Sturm, SPIE 2248 (1994) 50–62.
[49] Y.W. Kim, Fundamentals of analysis of solids by laser produced plasmas, in: L.J. Radziemski and D.A. Cremers (Eds.), Laser-Induced Plasmas and Applications, Marcel Dekker, Inc, New York (1989).
[50] a. H. Hegazy, E. AlAshkar, H. Abu Gabal, and N. Hamed, Temperature Evolution of Plasma Produced by Nd- YAG Laser, IEEE Transaction in Plasma Science V42 (2014) 1674-1684.
b. H. Hegazy, " Zinc Emission lines for Temperature Measurements of the Plasma Produced by Nano-second Laser", International Journal of Science and Research (IJSR), Volume 12, issue 12, (2023), pp.1353-1356.
[51] A. Ciucci, V. Palleschi, S. Rastelli, R. Barbini, F. Colao, R. Fantoni, A. Palucci, S. Ribezzo and H.J. van der Steen, Appl. Phys. B 63 (1996) 185–190.
[52] C. Aragon, J.A. Aguilera and F. Penalba, Appl. Spectrosc. 53 (1999) 1259-1267.
[53] M. Sabsabi and P. Cielo, J. Anal. At. Spectrom. 10 (1995) 643-647.
[54] F. Leis, W. Sdorra, J.B. Ko, K. Niemax, Microchim. Acta II (1989) 185-199.
[55] K.J. Grant and G.L. Paul, Applied Spectroscopy 44 (1990) 1349-1354.
[56] W. Sdorra and K. Niemax, Microchim. Acta 107 (1992) 319–327.
[57] Y. Iida, Spectrochim. Acta Part B 45 (1990) 1353-1367.

[58] D.E. Kim, K.J. Yoo, H.K. Park, K.J. Oh and D.W. Kim, Appl. Spectrosc. 51 (1997) 22-29.
[59] J. Hermann, C. Boulmer Leborgne and D. Hong, J. Appl. Phys. 83 (1998) 691-696.
[60] T.L. Thiem, R.H. Salter, J.A. Gardner, Y.I. Lee and J.Sneddon, Appl. Spectrosc. 48 (1994) 58-64.
[61] Shudi Zhang, Xiaohua Wang, Miaohong He, Yunbin Jiang, Bochao Zhang, Wei Hang, Benli Huang, Spectrochim. Acta Part B 97 (2014) 13–33.
[62] P. Stavropoulos, C. Palagas, G.N. Angelopoulos, D.N. Papamantellos, S. Couris, "Calibration Measurements in laser-induced breakdown spectroscopy using nanosecond and picosecond lasers", Spectrochim. Acta Part B: At. Spectrosc. 59 (2004) 1885-1892
[63] Y.-I. Lee, K. Song, H.-K. Cha, J.-M. Lee, M.-C. Park, G.-H. Lee, J. Sneddon, "Influence of atmosphere and irradiation wavelength on copper plasma emission induced by excimer and Q-switched Nd: YAG laser ablation", Appl. Spectrosc. 51 (1997) 959-964.
[64] Y.-I. Lee, S.P. Sawan, T.L. Thiem, Y.-Y. Teng, J. Sneddon, "Interaction of a laser beam with metals. Part II: Space-resolved studies of laser-ablated plasma emission", Appl. Spectrosc. 46 (1992) 436-441.
[65] J.A. Aguilera, C. Aragón, "Multi-element Saha–Boltzmann and Boltzmann plots in laser-induced plasmas", Spectrochim. Acta Part B: At. Spectrosc. 62 (2007) 378-385.
[66] H. Hegazy, H.A. Abd El-Ghany, S.H. Allam, T.M. El-Sherbini, "Spectral evolution of nano-second laser interaction with Ti target in Air", Appl. Phys. B: Lasers and Optics 110 (2013) 509-518.
[67] S.Y. Moon, W. Choe, Spectrochim. Acta Part B: At. Spectrosc. 58 (2003) 249-257.
[68] S.S. Harilal, R.C. Issac, C.V. Bindhu, P. Gopinath, V.P.N. Nampoori, C.P.G. Vallabhan, Spectrochim. Acta Part A: Mol. Spectrosc. 53 (1997) 1527-1536.
[69] J.A. Van der Mullen, Phys. Rep. Phys. Let, PRPLCM 191 (2 and 3) 109-220 (1990).
[70] H. Hegazy, E. A. Abdel-Wahab , F. M. Abdel-Rahim, S.H. Allam , and A. M A. Nossair , "Evaluation of Plasma Produced by First and Second Harmonic Nano-Second Laser for Enhancing the Capability of Laser Induced Breakdown Spectroscopy Technique" Eur. Phys. J.D. V 68 (2014) 107.
[71] S.S. Harilal, B. O'Shay, M.S. Tillack, M.V. Mathew, J. Appl. Phys. 98 (2005) 013306.
[72] J.A. Aguilera, C. Aragón, Spectrochim. Acta Part B: At. Spectrosc. 59 (2004) 1861-1876.
[73] M. Sabsabi, P. Cielo, Appl. Spectrosc. 49 (1995) 499-507.
[74] J.B. Simeonsson, A.W. Miziolek, Appl. Opt. 32 (1993) 939-947.
[75] L.J. Radziemski, T.R. Loree, D.A. Cremers, N.M. Hoffman, Anal. Chem. 55 (1983) 1246-1252.
[76] R. Qindeel, M.S. Dimitrijević, N.M. Shaikh, N. Bidin, Y.M. Daud, Eur. Phys. J. Appl. Phys. 50 (2010) 30701.
[77] M. Adamson, A. Padmanabhan, G.J. Godfrey, S.J. Rehse, Spectrochim. Acta Part B: At. Spectrosc. 62 (2007) 1348-1360.
[78] H. Hegazy, H.A. Abd El-Ghany , S.H. Allam, and Th. M. El-Sherbini, "Spectral Evolution of Nano-Second Laser Interaction with Ti Target in Nitrogen Ambient Gas, Appl. Phys. B: Lasers and Optics, accepted 09 April 2014, Online 7 May 2014.
[79] H. Hegazy, "O I Spectral Lines for Diagnostics of Atmospheric Laser Induced Plasmas", Appl. Phys. B: Lasers and Optics V 98 (2010) 601–606.
[80] H. Hegazy, F.M. Abdel-Rahim, S.H. Allam, "Evolution of Al plasma generated by Nd–YAG laser radiation at the fundamental wavelength", Appl. Phys. B: Lasers and Optics 108 (2012) 665-673.
[81] H. Hegazy, "Copper Emission lines for Temperature Measurements of the Plasma Produced by Nano-second Laser", Arab Journal for Nuclear Sciences and Applications V 47 (2014) 107-113.
[82] N.M. Shaikh, B. Rashid, S. Hafeez, S. Mahmood, M.A. Saleem, M. Baig, J. Appl. Phys. 100 (2006) 073102.
[83] N.M. Shaikh, S. Hafeez, B. Rashid, S. Mahmood, M.A. Baig, J. Phys.D: Appl. Phys. 39 (2006) 4377-4385.
[84] W.F. Luo, Q.B. Sun, C.X. Gao, J. Tang, H.J. Wang, W. Zhao, Plasma Sci. Technol. 12 (2010) 385-390.
[85] C. Colón, G. Hatem, E. Verdugo, P. Ruiz, J. Campos, J. Appl. Phys. 73 (1993) 4752-4758.
[86] N.M. Shaikh, B. Rashid, S. Hafeez, S. Mahmood, M.A. Saleem, M. Baig , J. Appl. Phys. 100 (2006) 073102.
[87] G. Cristoforetti, G. Lorenzetti, S. Legnaioli, V. Palleschi, Spectrochim. Acta Part B: At. Spectrosc. 65 (2010) 787-796.
[88] A.M. El Sherbini, T.M. El Sherbini, H. Hegazy, G. Cristoforetti, S. Legnaioli, V. Palleschi, L. Pardini, A. Salvetti, E. Tognoni, Spectrochim. Acta Part B: At. Spectrosc. 60 (2005) 1573-1579.
[89] I.B. Gornushkin, J.M. Anzano, L.A. King, B.W. Smith, N. Omenetto, J.D. Winefordner, Spectrochim. Acta Part B: At. Spectrosc. 54 (1999) 491-503.
[90] C. Aragón, F. Peñalba, J.A. Aguilera, Spectrochimica Acta Part B: At. Spectrosc. 60 (2005) 879-887.
[91] D.W. Hahn, N. Omenetto, Appl. Spectrosc. 64 (2010) 335A-366A.
[92] J. Hermann, A. Thomann, C. Boulmer-Leborgne, B. Dubreuil, M. De Giorgi, A. Perrone, A. Luches, N. Mihailescu, J. Appl. Phys. 77, (1995) 2928–2936.
[93] P. Stavropoulos, C. Palagas, G.N. Angelopoulos, D.N. Papamantellos and S. Couris, Spectrochimica Acta Part B 59 (2004) 1885-1892.
[94] S.S. Harilal, Appl. Opt. 43 (2004) 3931-3937.
[95] C.Y. Diao, C.S. Chen, B.Y. Man, C. Wang, H.B. Fu, Eur. Phys. J. D 63 (2011) 123-128.
[96] H.S. Park, S.H. Nam, S.M. Park, J. Appl. Phys. 97 (2005) 113103.
[97] F. Colao, R. Fantoni, V. Lazic, A. Paolini, Appl. Phys. A 79 (2004) 143-152.
[98] J.S. Cowpe, J.S. Astin, R.D. Pilkington, A.E. Hill, Spectrochim. Acta Part B: At. Spectrosc. 63 (2008) 1066-1071.
[99] N.M. Shaikh, Y. Tao, R.A. Burdt, S. Yuspeh, N. Amin, M.S. Tillack, J. Appl. Phys. 108 (2010) 083109.
[100] D.A. Cremers, L.J. Radziemski, T.R. Loree, Appl. Spectrosc. 38 (1984) 721-729.

[101] J. Hermann, C. Boulmer-Leborgne, D. Hong, J. Appl. Phys. 83 (1998) 691-696.
[102] L.J. Radziemski, T.R. Loree, D.A. Cremers and N.M. Hoffman, Anal. Chem. 55 (1983) 1246–1252.
[103] S.S. Harilal, C.V. Bindhu, R.C. Isaac, V.P. Nampoori and C.P. Vallabhan, J. Appl. Phys. 82 (1997) 2140–2146.
[104] H.C. Liu, X.L. Mao, J.H. Yoo, and R.E. Russo, Spectrochim. Acta B 54 (1999) 1607.
[105] X. Zeng, X.L. Mao, S. Mao, J.H. Yoo, R. Greif, and R.E. Russo, J. Appl. Phys. 95 (2004) 816.
[106] T. Wujec, J. Halenka, A. Jazgara and J. Musielok, J. Quant. Spectrosc. & Rad. Transf. 74 (2002) 663–666.
[107] A. M. El Sherbini, H. Hegazy, and Th. M. El Sherbini, "Measurement of Electron Density Utilizing the H□-Line from Laser Produced Plasma in Air", Spectrochim. Acta Part B: At. Spectrosc. 61, 532-539 (2006).
[108] C. Colon, G. Hatem, E. Verdugo, P. Ruiz, and J. Campos, J. Appl. Phys. 73 (1993) 4752.
[109] H.R. Griem, Spectral Line Broadening by Plasmas, Academic Press, New York, 1974.
[110] J. Ashkenazy, R. Kipper, M. Caner, "Spectroscopic measurements of electron density of capillary plasma based on Stark broadening of hydrogen lines", Phys. Rev. A 43 (1991) 5568–5574.
[111] V. Detalle, Rene Heon, M. Sabsabi, and L. St-Onge, Spectrochim. Acta Part B: At. Spectrosc. 56 (2001) 1011-1025.
[112] L. J. Radziemski, "Review of selected analytical applications of laser plasmas and laser ablation", Microchem J. 50 (1994) 218-234.
[113] D. W. Hahn, W. L. Flower, and K. R. Hencken, Appl. Spectrosc. 51 (1997) 1836-1844.
[114] W.T.Y. Mohamed, "Quantitative elemental analysis of seawater by laser induced breakdown spectroscopy", Int. J Pure Appl. Phys. 2 (2006) 11-21.
[115] K. Song, Y.-I. Lee, J. Sneddon, "Recent developments in instrumentation for laser-induced breakdown spectroscopy", Appl. Spectrosc. Rev. 37 (2002) 89-117.
[116] E. Tognoni, V. Palleschi, M. Corsi, G. Cristoforetti, "Quantitative microanalysis by laser-induced breakdown spectroscopy: a review of the experimental approaches", Spectrochim. Acta Part B 57 (2002) 1115-1130.
[117] D. A. Cremers, "The Analysis of Metals at a Distance Using Laser-Induced Breakdown Spectroscopy", Appl. Spectrosc. 41.(1987) 572.
[118] M. Sabsabi, V. Detalle, M.A. Harith, W. Tawfik, H. Imam, "Comparative study of two new commercial Echelle spectrometers equipped with intensified CCD for analysis of laser-induced breakdown spectroscopy", Appl Opt. 42 (2003) 6094-6098.
[119] M.A. Ismail, H. Imam, A. Elhassan, W. T. Youniss, M.A. Harith, "LIBS limit of detection and plasma parameters of some elements in two different metallic matrices", J. Anal. At. Spectrom. 19 (2004) 489-494.
[120] P. Fichet, A. Toussaint, J.F. Wagner, "Laser-induced breakdown spectroscopy: a tool for analysis of different types of liquids", Appl. Phys. A 69 (1999) pp. 591-592.
[121] P. Fichet, P. Mauchien, J.F. Wagner, C. Moulin, "Quantitative elemental determination in water and oil by laser induced breakdown spectroscopy", Anal. Chim. Acta 42 (2001) 269-278.
[122] D. A. Rusak, B. C. Castle, B. W. Smith, J. D. Winefordner, "Fundamentals and applications of laser-induced breakdown spectroscopy", Crit. Rev. Anal. Chem. 27 (1997) 257-290.
[123] J. Sneddon, Y-I. Lee, "Novel and recent applications of elemental determination by laser-induced breakdown spectrometry", Anal. Lett. 32 (1999) 2143-2162.
[124] V. Majidi, M. R. Joseph, "Spectroscopic applications of laser-induced plasmas", Crit Rev. Anal. Chem. 23 (1992) 143-162.
[125] A. Ciucci, M. Corsi, V. Palleschi, S. Rastelli, A. Salvetti, E. Tognoni, "A new procedure for quantitative elemental analyses by laser induced plasma spectroscopy". Appl. Spectrosc. 53 (1999) 960-964.
[126] E. H. Piepmeier, "Laser ablation for atomic spectroscopy, analytical application of laser". New York, Wiley; (1986).
[127] H.E. Bauer, F. Leis, K. Niemax, "Laser induced breakdown spectrometry with an echelle spectrometer and intensified charge coupled device detection". Spectrochim. Acta Part B 53 (1998) 1815-1825.
[128] R.E. Russo, X.L. Mao, "Chemical analysis by laser ablation". In: J.C. Miller, R.F. Haglund, editors. "Laser Experimental Ablation and Desorption". San Diego, Academic Press; pp. 375 (1998).
[129] K.Y. Yamamoto, D.A. Cremers, M.J. Ferris, L.E. Foster, "Detection of metals in the environment using a portable laser-induced breakdown spectroscopy instrument". Appl. Spectrosc. 50 (1996) 222-233.
[130] B.C. Castle, K. Talabardon, B.W. Smith, J.D. Winefordner, "Variables influencing the precision of laser-induced breakdown spectroscopy measurements". Appl. Spectrosc. 52 (1998) 649-657.
[131] Yu-Fang Yueh, J.P. Singh, H. Zhang, "Laser-induced Breakdown Spectroscopy: Elemental Analysis". In: R.A. Meyers, editor. Encyclopedia of Analytical Chemistry. Chichester: Wiley; pp. 2066-2087 (2000).
[132] V. Bulatov, R. Krasniker, I. Schechter, "Study of matrix effects in laser plasma spectroscopy by combined multi-fiber spatial and temporal resolutions". Anal. Chem. 70 (1998) 5302-5310.
[133] K.L. Eland, D.N. Stratis, D.M. Gold, S.R. Goode, S. Michael Angel "Energy dependence of emission intensity and temperature in a LIBS plasma using femtosecond excitation", Appl. Spectrosc. 55 (2001) 286-291.
[134] A. Semerok, C. Chale´ard, V. Detalle, J.L. Lacour, P. Mauchien, P. Meynadier, C. Nouvellon, B. Salle´, P. Palianov, M. Perdrix, G. Petite "Experimental investigations of laser ablation efficiency of pure metals with femto, pico and nanosecond pulses", Appl. Surf. Sci. 138-139 (1999) 311-314.
[135] L. Xu, V. Bulatov, V. Gridin, I. Schechter, "Absolute analysis of particulate materials by laser-induced breakdown spectroscopy". Anal. Chem. 69 (1997) 2103-2108.

[136] S.R. Goode, S.L. Morgan, R. Hoskins, A. Oxsher, "Identifying alloys by laser-induced breakdown spectroscopy with a time-resolved high resolution echelle spectrometer". J. Anal. At. Spectrom. 15 (2000) 1133-1138.
[137] A.S. Eppler, D.A. Cremers, D.D. Hickmott, M.J. Ferris, A.C. Koskelo, "Matrix effects in the detection of Pb and Ba in soils using laser induced breakdown spectroscopy". Appl. Spectrosc. 50 (1996) 1175-1181.
[138] K. Meissner, T. Lippert, A. Wokaun, K. Guenther, "Analysis of trace metals in comparison of laser-induced breakdown spectroscopy with LA-ICP-MS", Thin Solid Films 453–454 (2004) 316–322.
[139] G. Cristoforetti, S. Legnaioli, L. Pardini, V. Palleschi, A. Salvetti, E. Tognoni, "Spectroscopic and shadowgraphic analysis of laser induced plasmas in the orthogonal double pulse pre-ablation configuration", Spectrochim. Acta Part B 61 (2006) 340–350.
[140] K. Amal, S.H. Elnaby, V. Palleschi, A. Salvetti, M.A. Harith, "Comparison between single and double-pulse LIBS at different air pressures on silicon target", App. Phys. B: Lasers and Optics 83 (2006) 651–657.
[141] C. Sánchez-Aké, Marduk Bolaños , C.Z. Ramírez, "Emission enhancement using two orthogonal targets in double pulse laser-induced breakdown spectroscopy", Spectrochim. Acta Part B 64 (2009) 857-862.
[142] G. Cristoforetti, "Orthogonal double-pulse versus single-pulse laser ablation at different air pressures: a comparison of the mass removal mechanisms", Spectrochim. Acta Part B 64 (2009) 26–34.
[143] H. Hegazy, E. A. Abdel-Wahab , F. M. Abdel-Rahim, S.H. Allam , and A. M A. Nossair , "Laser induced breakdown spectroscopy: technique, new features, and detection limits of trace elements in Al base alloy", Appl. Phys. B: Lasers and Optics 115 (2014) 173–183.
[144] H. Hegazy, E. A. Abdel-Wahab, F. M. Abdel-Rahim, S. H. Allam, A. M. A. Nossair, "Laser induced breakdown spectroscopy using a second harmonic nano-second laser and enhancements the detection limits of trace elements in Al base alloy", Arab Journal of Nuclear Science and Applications 47 (2014) 80-92.
[145] Li Hong-kun, Liu Ming, Chen Zhi-jiang and Li Run-hua, Trans. Nonferrous Met. Soc. China 18 (2008).
[146] M. A. Ismail, S. Legnaioli, V. Palleschi, E. Tognoni, G. Cristofretti, L. Pardini, A. Salvetti and M. A. Harith J. Anal. Bioanal. Chem. 385 (2006) 316-325.
[147] B. Le Drogoff, J. Margot,T.W. Johnston, M. Chaker, S. Laville, M. Sabsabi, F. Vidal, O. Barthelemy, Y. von Kaenel, Spectrochim. Acta Part B 56 (2001) 987 -1002.
[148] W. T. Y. Mohamed, Optics& Laser Technology 40 (2008) 30-38.
[149] B. Nemet, L. Kozma, Spectrochim. Acta Part B 50 (1995) 1869-1888.
[150] D. Body, B.L. Chawick, Spectrochim. Acta Part B 56 (2001) 725-736.
[151] M. Sabsabi, R. Heon, L. St-Onge, Spectrochim. Acta Part B 60 (2005) 1211–1216.
[152] L. Fornarini, V. Spizzichino, F. Colao, R. Fantoni, V. Lazic, Influence of laser wavelength on LIBS diagnostics applied to the analysis of ancient bronzes, Anal. Bioanal. Chem. 385 (2006) 272–280.
[153] H. Hegazy, "Improving the Limit of Detection in Laser-Induced Breakdown Spectroscopy and Measuring the Associated Plasma Parameters", International Journal of Science and Research (IJSR), Volume 13 Issue 5, (2024) pp. 1910-1915.
[154] J. B. Olsen, J. H. Macedone and P B. Farnsworth, J. Anal. At. Spectrom. 21 (2006) 856-860.
[155] P. Serapinas, J. Salkauskas, Z. Ezerinskis and A. Acus, Spectrochim. Acta Part B: Atomic Spectroscopy 65 (2010) 15–23.
[156] Ž. Andreić, D. Gracin, V. Henč-Bartolić, H.-J. Kunze, F. Ruhl, L. Aschke., "Dynamics of laser-produced carbon plasma", Physica Scripta 53 (1996) 339.
[157] B. Toftmann, J. Schou, and J. G. Lunney, "Dynamics of the plume produced by nanosecond ultraviolet laser ablation of metals", Phys. Rev. B 67 (2003).104101.
[158] B. Doggett, J. G. Lunney, "Expansion dynamics of laser produced plasma", J. Appl. Phys. 109 (2011) 093304.
[159] Sony George, Ph.D. Thesis, International School of Photonics Cochin University of Science & Technology, Cochin -682022, Kerala, India, (2011).
[160] R. K. Singh, Ajai Kumar, B. G. Patel, and K. P. Subramanian, Role of ambient gas and laser fluence in governing the dynamics of the plasma plumes produced by laser blow off of LiF–C thin film, J. Appl. Phys. 101 (2007) 103301.
[161] Sony George, Ajai Kumar, R. K. Singh, and V. P. N. Nampoori, Fast imaging of laser-blow-off plume: Lateral confinement in ambient environment, Appl. Phys. Lett. 94 (2009) 141501.
[162] Bhupesh Kumar, R K Singh, and Ajai Kumar, Dynamics of laser-blow-off induced Li plume in confined geometry, Phys. Plasmas 20 (2013) 083511.
[163] J. F. Friichtenilht, "Laser generated pulsed atomic beams", Rev. Sci. Instrum. 45 (1974) 51.
[164] X. K. Shen, Y. F. Lu, T. Gebre, H. Ling, and Y. X. Han, J. Appl. Phys. 100 (2006) 053303.
[165] T. Shirai, Y. Funatake, K. Mori, J. Sugar, and W. L. Wiese, "Spectral data and Grotrian diagrams for highly ionized iron, Fe viii-xxvi", J. Phys. Chem. Ref. Data 19 (1990) 127.
[166] Y.-K. Kim, D. H. Baik, P. Indelicato, and J. P. Desclaux, "Resonance transition energies of Li-, Na-, and Cu-like ions," Phys. Rev. A 44 (1991) 148.
[167] O. Marchuk. PhD thesis, Ruhr-Universität Bochum, (2004).
[168] D. Zhao et al., Remote in situ laser-induced breakdown spectroscopic approach for diagnosis of the plasma facing components on experimental advanced superconducting tokamak. Rev. Sci. Instrum. 89 (2018) 073501.
[169] G. S. Maurya, A. Marín-Roldán, P. Veis, A. K. Pathak, and P. Sen, "A review of the LIBS analysis for the plasma-facing components diagnostics". J. Nucl. Mater. 541 (2020) 152417.
[170] E. Tognoni, G. Cristoforetti, S. Legnaioli, V. Palleschi, "Calibration-Free Laser-induced Breakdown Spectroscopy: State of the Art", Spectrochimica Acta Part B: Atomic Spectroscopy 65 (2010) 1–14.

[171] W. Wei, J. Wu, X. Li, S. i. Jia, and A. Qiu, J. of Appl. Phys. 114 (2013) 113304.
[172] S. B. Wen, X. L. Mao, R. Greif, and R. E. Russo, J. Appl. Phys. 101 (2007) 023114.
[173] S. S. Harilal, G. V. Miloshevsky, P. K. Diwakar, N. L. LaHaye, and A. Hassanein, Phys. Plasmas 19 (2012) 083504.
[174] K. R. Chen, T. C. King, J. H. Hes, J. N. Leboeuf, D. B. Geohegan, R. F. Wood, A. A. Puretzky, and J. M. Donato, Phys. Rev. B 60 (1999) 8373.
[175] N. Farid, S. S. Harilal, H. Ding, and A. Hassanein, J. Appl. Phys. 115 (2014) 033107.
[176] V. Palleschi, S. Legnaioli, F. Poggialini, F. et al., "Laser-induced breakdown spectroscopy", Nat Rev Methods Primers 5, (2025) 17. https://doi.org/10.1038/s43586-025-00388-w.